The OLYMPUS Experiment

N. Akopov[m], R. Alarcon[a], V.A. Andreev[j], O. Ates[d], A. Avetisyan[m], R. Beck[c], S. Belostoski[j], J.C. Bernauer[i], F. Brinker[b], J.R. Calarco[l], V. Carassiti[f], E. Cisbani[g], G. Ciullo[f], M. Contalbrigo[f], N. D'Ascenzo[b], R. De Leo[e], J. Diefenbach[d,h], T.W. Donnelly[i], K. Dow[i], G. Elbakian[m], P.D. Eversheim[c], S. Frullani[g], Ch. Funke[c], G. Gavrilov[j], B. Glaeser[h], N. Goerrissen[b], D.K. Hasell[i,*], J. Hauschildt[b], B. Henderson[i], Ph. Hoffmeister[c], Y. Holler[b], L.D. Ice[a], A. Izotov[j], R. Kaiser[k], G. Karyan[m], J. Kelsey[i], D. Khaneft[h], A. Kiselev[j], M. Kohl[d], A. Krivshich[j], I. Lehmann[k], P. Lenisa[f], D. Lenz[b], S. Lumsden[k], Y. Ma[h], F. Maas[h], H. Marukyan[m], O. Miklukho[j], R. Milner[i], A. Movsisyan[f,m], M. Murray[k], Y. Naryshkin[j], C. O'Connor[i], R. Perez Benito[h], R. Perrino[e], R.P. Redwine[i], D. Rodríguez Piñeiro[h], G. Rosner[k], R. Russell[i], A. Schmidt[i], H. Schmieden[c], U. Schneekloth[b], B. Seitz[k], M. Statera[f], H. Vardanyan[m], D. Veretennikov[j], C. Vidal[i], A. Winnebeck[i], V. Yeganov[m]

[a] *Arizona State University, Tempe, AZ, USA*
[b] *Deutsches Elektronen-Synchrotron, Hamburg, Germany*
[c] *Friedrich Wilhelms Universität, Bonn, Germany*
[d] *Hampton University, Hampton, VA, USA*
[e] *Istituto Nazionale di Fisica Nucleare, Bari, Italy*
[f] *Universita' di Ferrara and Istituto Nazionale di Fisica Nucleare, Ferrara, Italy*
[g] *Istituto Nazionale di Fisica Nucleare, Rome, Italy*
[h] *Johannes Gutenberg Universität, Mainz, Germany*
[i] *Massachusetts Institute of Technology, Cambridge, MA, USA*
[j] *Petersburg Nuclear Physics Institute, Gatchina, Russia*
[k] *University of Glasgow, Glasgow, United Kingdom*
[l] *University of New Hampshire, Durham, NH, USA*
[m] *Yerevan Physics Institute, Yerevan, Armenia*

Abstract

The OLYMPUS experiment was designed to measure the two-photon contribution in elastic electron-proton scattering. Two-photon exchange could

*Corresponding Author
Email address: hasell@mit.edu (D.K. Hasell)

explain the discrepancy between measurements of the form factor ratio, $\mu_p G_E^p/G_M^p$, made using polarization techniques and those made in unpolarized experiments. To achieve its goal, OLYMPUS operated on the DORIS storage ring at DESY with electron and positron beams at 2.01 GeV incident on an internal hydrogen gas target to determine the ratio of elastic scattering cross sections for positrons versus electrons. The experiment used a toroidal magnetic spectrometer instrumented with drift chambers and time of flight detectors to measure rates for elastic scattering over the polar angular range of approximately 25°–75°. A symmetric Møller / Bhabha calorimeter and telescopes of GEM and MWPC detectors at 12° served as luminosity monitors. A total luminosity of ~ 4.5 fb^{-1} was collected. This paper provides details on the accelerator, target, detectors, and operation of the experiment.

Keywords: elastic electron scattering, elastic positron scattering, two-photon exchange, form-factor ratio
2010 MSC: 25.30.Bf, 25.30.Hm, 13.60.Fz, 13.40.Gp, 29.30.-h

1. Introduction

The structure of nucleons has long been studied using electromagnetic probes. Point-like electrons and positrons are ideal for this since the lepton vertex is well described by quantum electro-dynamics. The mediating photon (or weak boson at higher energies) can be used to "see" deeper and deeper into the nucleon. As the momentum transfer increases, the measurements progress from the nucleon size to the elastic form factors, G_E and G_M, arising from the distribution of charge and magnetism inside the nucleon. At still higher momentum transfers, deep inelastic scattering reveals the distributions of the quarks and gluons that ultimately must produce the observed form factors and nucleon sizes. The resulting data can then be used to verify our theoretical understanding of the innermost workings of the nucleon. With polarized beams and targets, even more details are available.

Recently, measurements of the electric to magnetic form factor ratio, $\mu_p G_E^p/G_M^p$, using polarization techniques (1–8) have shown a dramatic discrepancy in comparison with the ratio obtained using the traditional Rosenbluth technique in unpolarized cross section measurements (9–12) as shown in Fig. 1. This discrepancy has been explained as arising from multiple-photon exchange beyond the usual one-photon exchange. Since most of our understanding on the structure of the proton has assumed a single mediating photon, it is essential to quantify the contribution of multiple-photon exchange and whether this explains the discrepancy or if there is some other contributing process.

To address this question, the OLYMPUS experiment was proposed to measure the ratio between the positron-proton and electron-proton elastic scattering cross sections. This ratio would be unity if only single photon exchange occurred. However, if multiple-photon exchange contributes significantly, the ratio will deviate from unity because the interference term between single- and double-photon exchange will change sign between electron and positron scattering. This ratio was measured in the 1960s with some indication of a deviation from unity but the uncertainties were large. This is shown in Fig. 2 together with some theoretical calculations and the projected OLYMPUS data.

The OLYMPUS proposal requested three months of dedicated operation on the DORIS electron/positron storage ring at the DESY laboratory in Hamburg, Germany. An unpolarized, hydrogen gas target was designed and built at MIT to be installed internally on the DORIS ring. To measure the

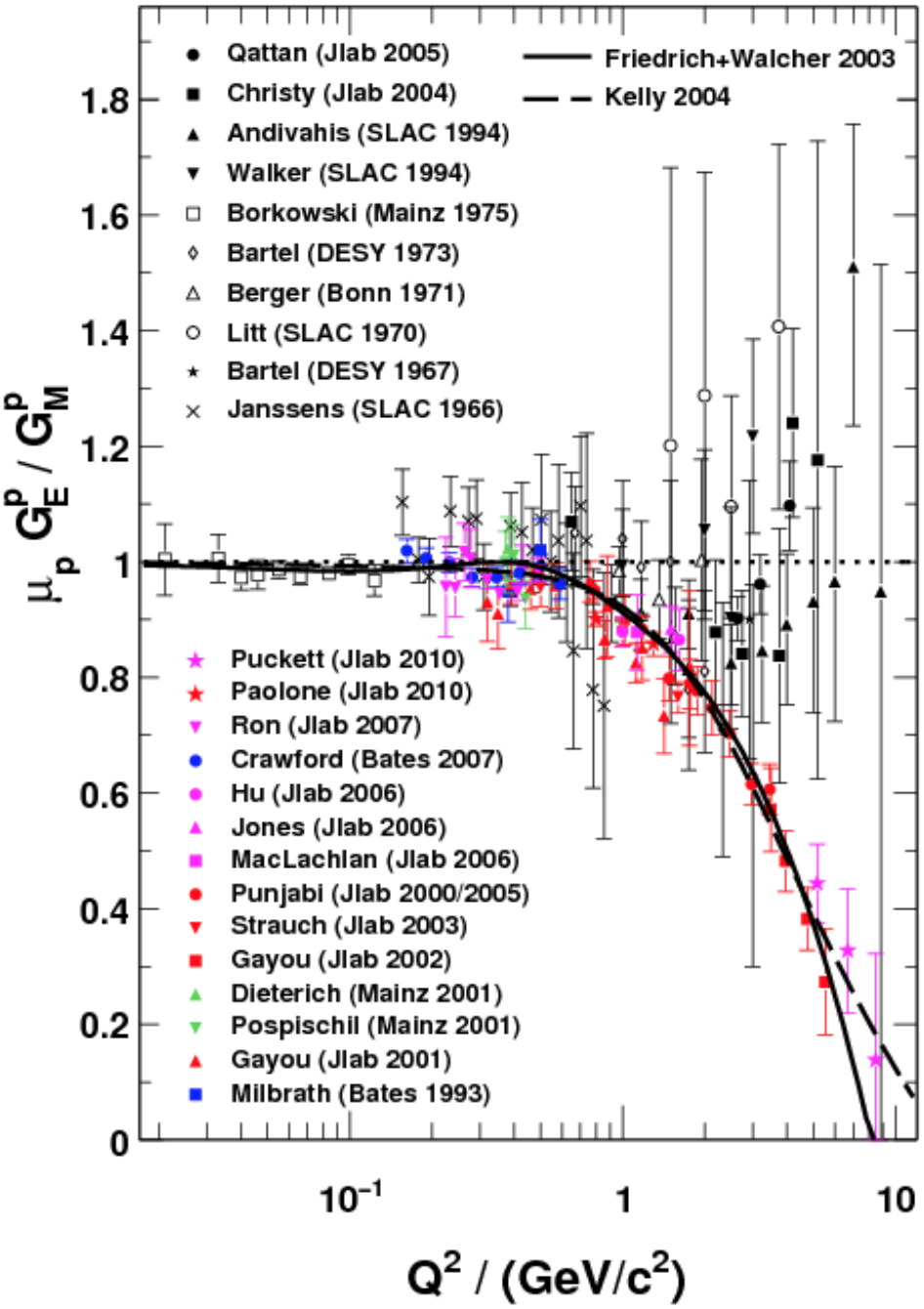

Fig. 1: Ratio of proton form factors $\mu_p G_E^p / G_M^p$ as a function of Q^2 showing results from unpolarized measurements in black and recent data measured using polarized techniques.

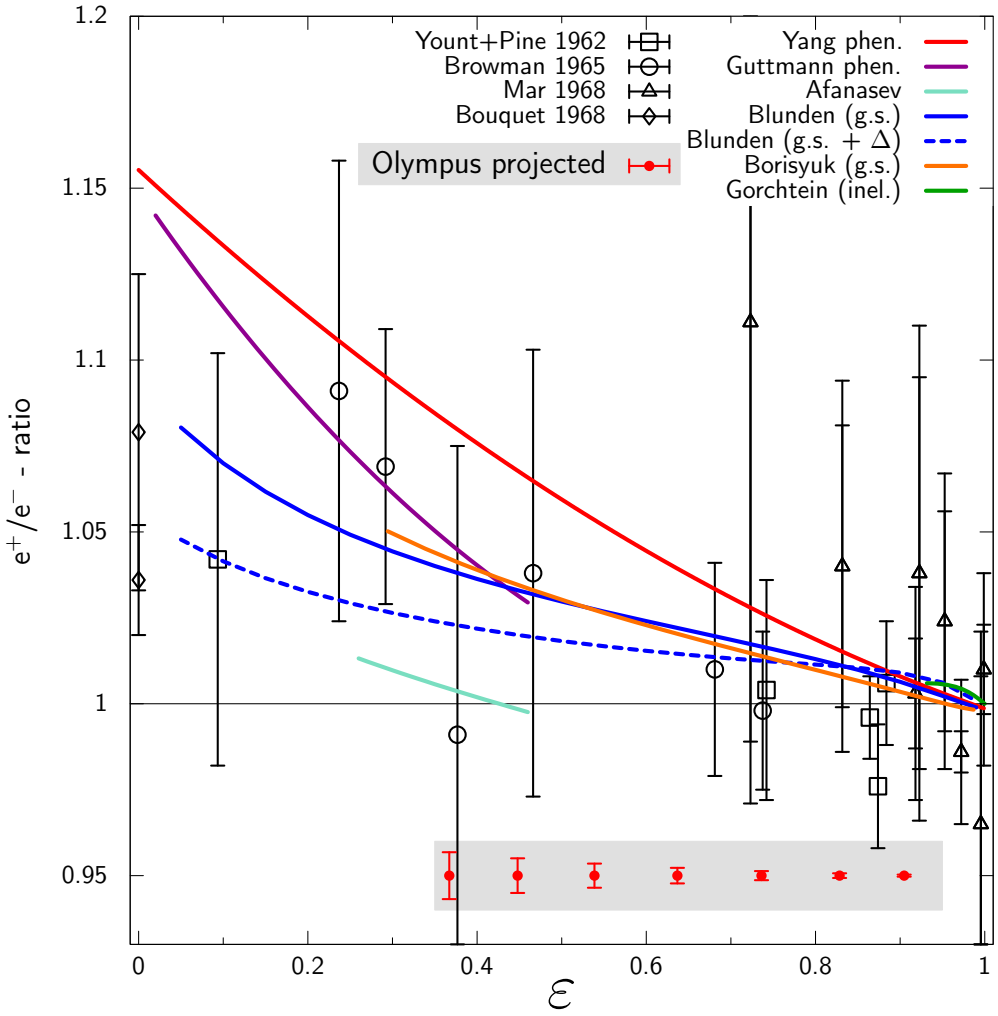

Fig. 2: Ratio of positron to electron elastic scattering cross section as a function of ϵ showing existing data, some theoretical predictions, and projected OLYMPUS data range and uncertainties.

ratio in elastic scattering cross sections, the former BLAST detector was shipped from MIT-Bates to DESY and installed on the DORIS ring. In addition, three new detector systems were designed and built to monitor the luminosity during the experiment. These were a symmetric Møller/Bhabha calorimeter from Mainz at 1.29° and telescopes of triple GEM detectors from Hampton and MWPC detectors from PNPI mounted at 12°. The data acquisition system was provided by the Bonn group. The trigger and slow control system were provided by MIT.

The following sections describe each of these systems in more detail.

2. DORIS Storage Ring at DESY

The DORIS storage ring at DESY in Hamburg was originally conceived in 1974 as an electron-electron and electron-positron collider. After its long and successful operation for particle physics research DORIS was dedicated to synchrotron radiation studies in 1993. In 2009 it was decided to shut down DORIS at the end of 2012 which put a very tight time constraint on the OLYMPUS experiment.

Since DORIS was designed to accelerate both electrons and positrons it was a natural choice for the OLYMPUS experiment. Also the location of the former ARGUS experiment was an excellent match to the size of the former BLAST detector.

Even though the DORIS accelerator and the ARGUS detector site were ideally suited for the OLYMPUS experiment several modifications had to be made to realize the experiment.

RF cavities that had been installed at the location of the former ARGUS detector had to be relocated 26 m upstream of the OLYMPUS interaction point..

Since it was impractical to remove the OLYMPUS target cell during synchrotron radiation runs the beam optics and lattice had to be modified to produce a waist in the beam at the OLYMPUS target center. At the same time the optical functions at the synchrotron radiation source points could not change significantly to allow continued operation of the optical beamlines. Especially the reduced beam size at the nearby HARWI wiggler (20 m downstream) had to be conserved The solution required an quadrupole on each side of the OLYMPUS interaction point, at $\pm$ 7 m.

The normal DORIS synchrotron operation used 4.5 GeV positrons with 150 mA in 5 bunches. The wakefield heating this produced necessitated cooling the OLYMPUS target cell even during the synchrotron operation.

OLYMPUS operated at 2.01 GeV with 10 bunches. This was a significant change for the normal DORIS operation and several studies and test periods were required with a multi-bunch feedback system before adequate currents and lifetimes were achieved.

One of the key features of the OLYMPUS experiment was the frequent switching between the particle polarities. The pre-accelerators, namely the linear accelerator, the accumulator ring and the DESY synchrotron are already able to switch between electrons and positrons within $\sim$ 10 minutes. But the extraction from the DESY synchrotron to DORIS, the transport

line, and the DORIS ring itself needed several modifications:

- The high voltage pulse forming power supplies for the DESY extraction and the DORIS injection kicker had to be rebuild.
- The septa magnets for the DESY extraction and DORIS injection were modified to serve as bipolar devices.
- Remotely controlled polarity switches for 24 magnet power supplies had to be built and installed 14 for 400 A and 10 for 800 A.

For powering the toroid of OLYMPUS a 7000 A DC power supply was needed. This was available at DESY but a 10 kV to 480 V transformer had to be installed near the DORIS hall and equipped with a 7000 A polarity switch. Cabling from the power supply to OLYMPUS had to be installed. The transformer also required water cooling. Similarly the OLYMPUS toroid magnet had to be water cooled so as to provide for both the "park" and "in-ring" positions,

Due to the frequent switching between electrons and positrons for OLYMPUS, parallel operation with the PETRA storage ring, which used the same pre-accelerators, was complicated. During the February data run PETRA was not operating and there was no conflict. For the later data period a fast-kicker was installed so PETRA could be filled in about 5 minutes.

Since the injection into DORIS happened at full energy it was possible to run in top-up mode and thus higher average currents and hence luminosity were possible. However, beam losses during injection had to be minimized to avoid tripping the OLYMPUS detectors. This was achieved plus slow control communication between the accelerator and the OLYMPUS data acquisition allowed the DAQ to be inhibited for approximately 100 ms around each injection pulse thus minimizing any lost time.

The gas target internal to the DORIS ring produced shorter beam lifetimes than normally experienced at DORIS. This corresponded to higher radiation downstream of the experiment. Additional shielding was required. Also the scrappers upstream of the experiment had to be optimized to minimize the noise rates in the experiment.

3. Target and Vacuum Systems

The OLYMPUS experiment used an unpolarized, internal hydrogen gas target cooled to around 40 K. The hydrogen gas flowed into an open-ended, 600 mm long, elliptical target cell (Sec. 3.1). The target cell was housed in a scattering chamber (Sec. 3.2) that had thin windows to match the angular acceptance of the detectors. A tungsten collimator (Sec. 3.4) was also housed in the scattering chamber to prevent synchrotron radiation, beam halo, and off-momentum particles from striking the target cell. Additionally, a series of wakefield suppressors (Sec. 3.3) were necessary to reduce the heat load on the target cell. Finally, an extensive vacuum system (Sec. 3.5) of turbomolecular and Non-Evaporable Getter (NEG) pumps was employed to preserve the vacuum in the DORIS storage ring.

3.1. Target Cell

The target cell consisted of an open-ended, elliptical cylinder (27 mm (horizontal)$\times$9 mm (vertical)$\times$600 mm long) made from 0.075 mm thick aluminum. The elliptical shape was chosen to match the DORIS beam envelope and was set to approximately ten times the nominal horizontal and vertical beam width at the OLYMPUS interaction point to minimize the amount of beam halo striking the cell walls.

Several target cells were made and tested before all the problems with heating, gas flow, and coupling to the wakefield suppressors were solved. A target cell (shown in Fig. 3) was formed from two identical, stamped sheets that were spot welded together along the top and bottom seams. The top seam was then clamped in an aluminum frame. The aluminum frame was connected, at its center, to a large copper block which was connected by a silver plated, laminated copper bar from Watteredge[1] to the cryogenic cold-head. A thin layer of indium was placed between all thermal connections to improve conductivity. The frame was made from 6063 aluminum to maximize thermal conductivity along the length of the cell, especially at cryogenic temperatures. The copper block was suspended from a flange in the top of the scattering chamber that permitted the height and angle of the target cell to be adjusted. The aluminum frame had temperature sensors mounted along its length and was wrapped in several layers of aluminized mylar to shield the target cell from thermal radiation.

[1]Watteredge, Inc. 567 Miller Road, Avon Lake, OH 44012, USA

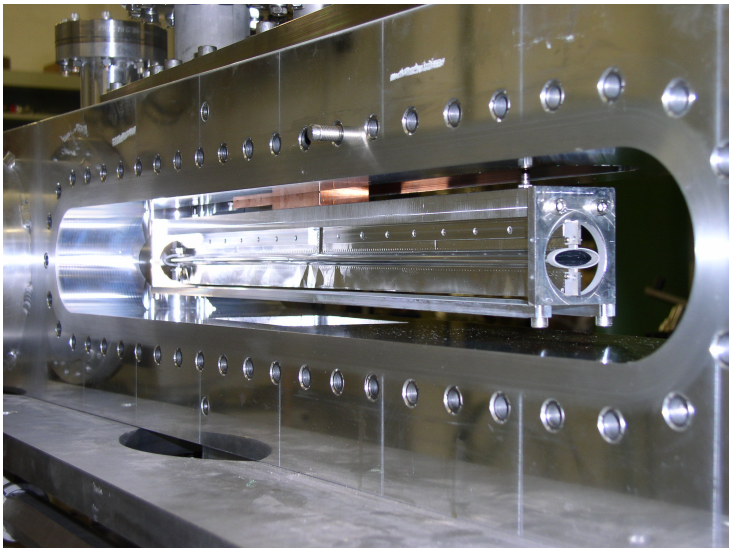

Fig. 3: Photograph of one of the OLYMPUS target cells mounted inside the scattering chamber.

Special elliptical rings were clamped around the target cell at either end. These were also coupled to the aluminum frame. The rings allowed the wakefield suppressors, up- and downstream of the target cell, to have good electrical contact to the target cell without damaging the delicate walls of the target cell. Care was taken to minimize any gaps or steps at this transition which would produce wakefield heating.

The hydrogen gas was produced by a commercial hydrogen generator. This electrolytically split water and filtered the resulting Hydrogen through a palladium membrane to achieve extremely high-purity ($\sim$ 99.9998%) hydrogen. The gas control system, shown schematically in Fig. 4, regulated the gas flow to the target cell by a series of valves, buffer volumes, and a mass flow controllers (MFCs). The hydrogen gas entered the target cell through a tube in the top flange of the scattering chamber. This tube fit snuggly inside a tubular opening stamped into the center of top seam of the target cell.

During operation, the hydrogen gas diffused slowly out the ends of the target cell and was pumped away by the vacuum system. The cell was cooled to reduce the temperature and diffusion of the gas in order to increase the target density. This resulted in a triangular, target density distribution with a maximum at the center of the target cell decreasing to zero at either end. A flow rate of 1.5×10^{17} H_2 atoms per second was required to produce a

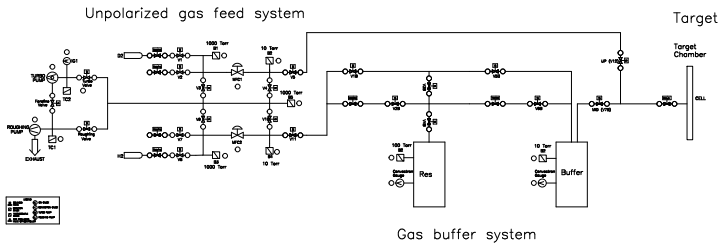

Fig. 4: Schematic of the unpolarized hydrogen gas system.

target thickness of 3×10^{15} atoms cm^{-2}.

3.2. Scattering Chamber

The OLYMPUS scattering chamber (shown in Fig. 5) is 1.5 m long and was machined from a solid block of aluminum. The trapezoidal shape was necessary for the detector telescopes at 12° to "see" most of the target cell through the windows. Ports for the beamline (up- and downstream), for pumping (on the bottom surface), and for access to the collimator (on the left and right) were welded to openings and fitted with ATLAS[2] explosion welded aluminum to stainless steel flanges so standard Conflat fittings could be used on the aluminum scattering chamber. O-ring seals were used on the top target cell flange and the two side windows.

The windows were 0.25 mm thick 1100 aluminum. These large area windows subtended a polar angular range of 8° to 100° from the center of the target, 6° to 90° from 200 mm upstream, and 10° to 120° from 200 mm downstream.

The top flange supported the target cell and the cold head that cooled the target cell. The cold head had to be shielded from the magnetic field with two layers of carbon steel to ensure efficient operation. A gas inlet flange fitted with a needle valve connected the hydrogen gas supply line to

[2]Atlas Technologies, 305 Glen Cove Road, Port Townsend, WA 98368, USA

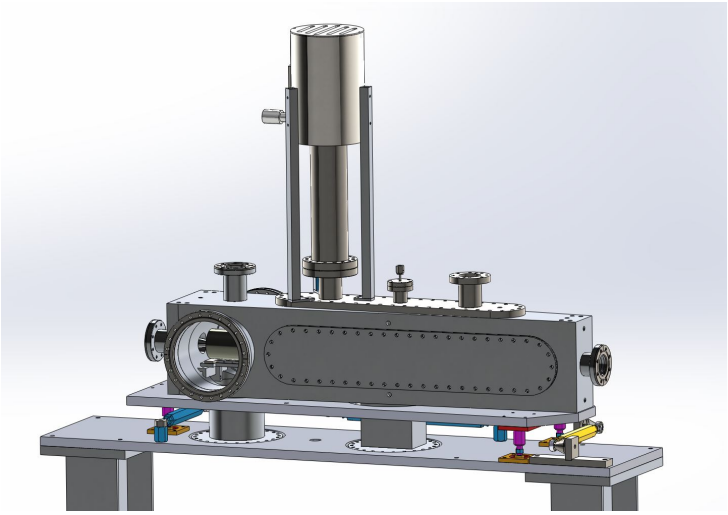

Fig. 5: CAD model of the OLYMPUS scattering chamber.

the target cell. An additional flange on the top held a multi-pin feedthrough for the numerous temperature sensors mounted along the target cell and on the wakefield suppressors.

The main components inside the scattering chamber are shown in Fig. 6,

3.3. Wakefield Suppressors

Wakefield suppressors were necessary to reduce the heating on the target cell from the circulating lepton beam. This allowed a temperature around 50 K to be maintained during operation with beam. To minimize the wakefield heating, changes in the beamline or cavity through which the lepton beam traveled had to be made gradually and any gaps or openings had to be minimized. Furthermore, it was crucial to maintain good electrical conductivity throughout. To achieve this, three wakefield suppressors were produced to cover the following transitions:

1. from the upstream 60 mm circular diameter beam pipe to the 25 mm by 7 mm elliptical opening of the collimator,
2. from the exit of the collimator to the entrance of the target cell (both 27 mm by 9 mm elliptical), and
3. from the 27 mm by 9 mm elliptical exit of the target cell to the 60 mm circular diameter of the down stream beamline.

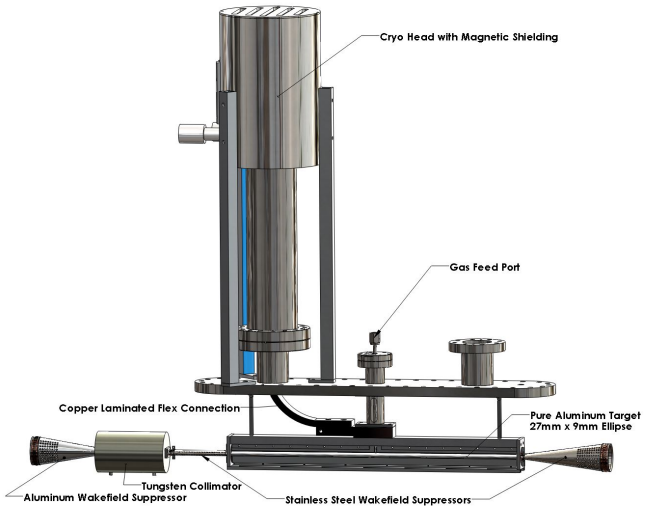

Fig. 6: CAD model of the target cell, wakefield suppressors, and collimator inside the OLYMPUS scattering chamber.

All three wakefield suppressors were silver plated for improved electrical conductivity. Also beryllium-copper, BeCu, spring fingers were attached around the circumferences to make a good, uniform electrical connection at each transition. These spring fingers also provided a sliding connection that allowed for thermal expansion.

The upstream wakefield suppressor was made from aluminum to have better thermal properties and to reduce the material thickness directly exposed to the beam. This piece was screwed directly to the collimator and made a sliding contact with the inside of the scattering chamber port that connected to the beam pipe.

The other two wakefield suppressors were made from stainless steel and were bolted to the rings on the target cell. This minimized the gap at the target cell. The BeCu spring fingers pressed against the target cell rings to make the electrical contact. The wakefield suppressor between the target cell and the collimator (see Fig. 7) made a sliding electrical connection to a elliptical spout screwed to the collimator. The suppressor downstream of the target cell made a sliding contact with the inside of the exit from the scattering chamber.

Each component was machined to the desired shape and numerous small holes were added to allow the target gas to be pumped away. The location

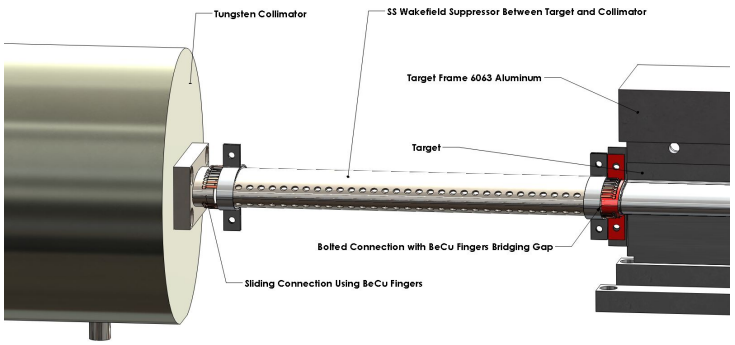

Fig. 7: CAD model of the wakefield suppressor between the collimator and the target cell.

of the holes was chosen to be as far as possible from the beam to reduce any wakefield effect.

3.4. Collimator

Fig. 5 also shows the fixed collimator in front of the target cell. The collimator consisted of a 140 mm long cylinder of tungsten 82.55 mm in diameter. The outer dimensions were chosen after performing a study on simulated showers of beam-halo particles. It had a tapered elliptical aperture with entrance 25 mm by 7 mm and exit 27 mm by 9 mm. This was machined from a solid block of tungsten using wire electrical discharge machining, EDM[3]. The entrance dimensions were chosen to be slightly smaller than those of the storage cell to shield the target cell walls.

3.5. Vacuum System

A system of magnetic levitation turbomolecular pumps[4] (800 l/s capacity) and NEG pumps[5] (400 l/s capacity) were used to pump the section of beamline inside the OLYMPUS experiment. This consisted of three stages of pumping to reduce the pressure from the relatively high pressure ($\sim 10^{-6}$ Torr) at the scattering chamber (caused by hydrogen gas) to the low pressure ($\sim 10^{-9}$ Torr) of the DORIS storage ring.

[3]Jack's Machine Co. Hanson, MA 02341
[4]Osaka and Edwards
[5]SAES Capacitor CFF 4H0402

The vacuum system is shown in Fig. 8. Two turbo pumps located in the

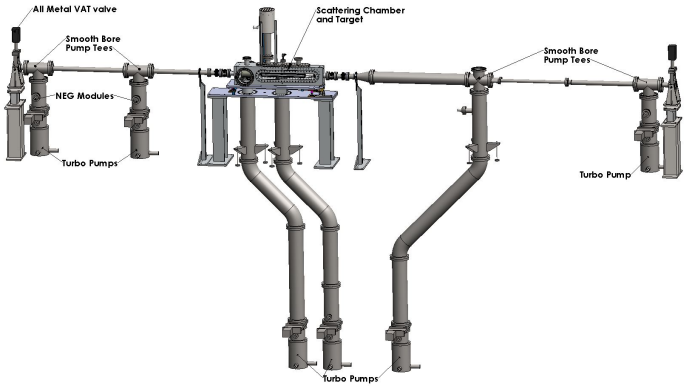

Fig. 8: CAD model of the vacuum system employed on the OLYMPUS experiment.

pit directly beneath the experiment were directly connected to the scattering chamber through 200 mm diameter pipes. Two more turbo pumps were connected to the up- and downstream beamlines approximately 2 m from the target. At approximately 3 m from the target another two turbo pumps were used to reduce the pressure in the beamline to the level acceptable for the DORIS storage ring. The four pumping stations furthest from the target also had NEG pumps to improve the ability for pumping hydrogen. The turbomolecular pumps were Osaka TG 1100M and Edwards STP 1003C.

4. The OLYMPUS Detector

The OLYMPUS detector used many of the components from the BLAST detector(13). The toroidal magnet, wire chambers, time of flight detectors, and much of the readout and control electronics from the BLAST experiment were shipped to DESY in the spring of 2010 and reassembled, with some modifications, to form the core of the OLYMPUS experiment.

The OLYMPUS experiment was situated on the south, straight section of the DORIS storage ring where the former ARGUS experiment(14) had been located. This was an ideal location for OLYMPUS as the ARGUS detector was comparable in size. The site consisted of a pit 7.2 m wide and 4.9 m below the beam height. The pit extended from inside the DORIS ring out to the DORIS hall. Two rails 3.2 m apart and 1.55 m high ran the length of the pit. Thus the OLYMPUS detector could be assembled on the rails outside the DORIS ring without interfering with the operation of DORIS. This was done from June, 2010 until July, 2011 at which time the shield wall was disassembled and OLYMPUS rolled into position. It was however necessary to modify the shield wall south and north of the "in-ring" detector position to allow the main frame of the OLYMPUS detector to open when necessary,

The pit also served as a convenient area, below the experiment, away from the toroidal magnetic field, to locate the roughing and turbo pumps, and the controls for the vacuum system. The target gas system, controls, cryopump, and the low voltage power supplies for the wire chambers were also placed beneath the experiment. However, while this was conveniently close to the experiment it was not accessible when DORIS was operating.

An electronics hut was also supported on the pit rail system and moved with the detector. However, the hut was outside the reassembled shielding wall and thus could be accessed even while beam was circulating in DORIS. This hut contained the readout and control electronics, high voltage power supplies, and the computers services for the experiment. It also provided a convenient work area during assembly and commissioning.

The gas system for the wire chambers were located in the pit beneath the electronics hut and could be accessed at all times. Gas systems for the GEM and MWPC detectors were located just outside the shielding wall in a corner of the DORIS hall floor.

The OLYMPUS experiment was based around an eight sector toroidal magnetic spectrometer. The two horizontal sectors were instrumented with

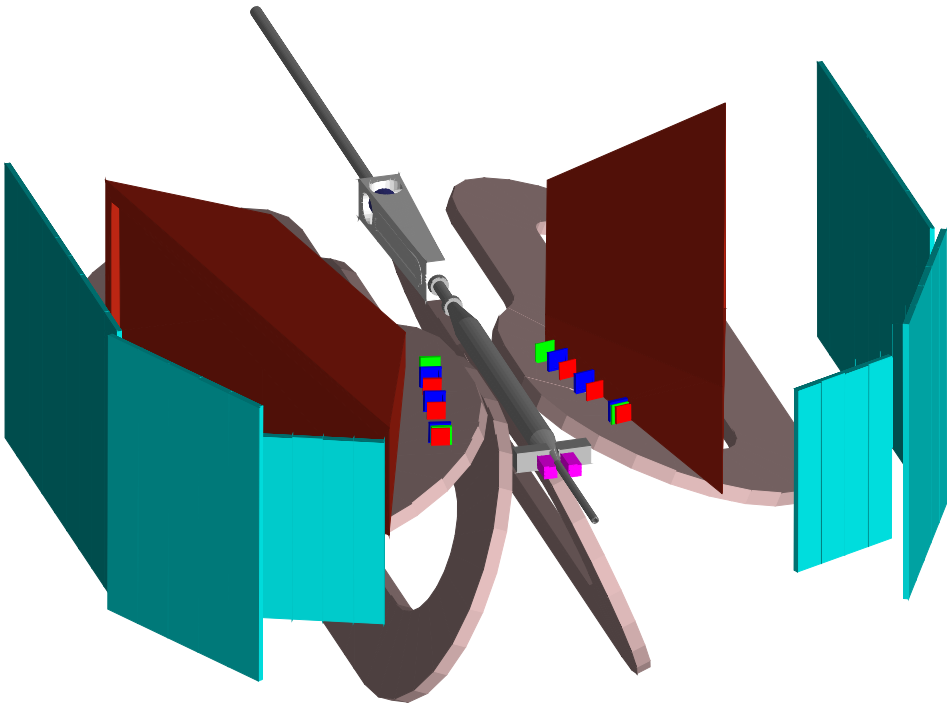

Fig. 9: Monte Carlo representation of the OLYMPUS detector with the top four magnet coils removed to show the instrumented horizontal sectors.

detectors to provide a roughly left/right symmetric system (see Fig. 9). Each sector consisted of wire chambers for tracking and momentum analyzing the reaction products. Behind the wire chambers were the time of flight scintillator bars which provided relative timing for the trigger and rough energy and position information. To monitor the experimental luminosity OLYMPUS had a redundant system of a symmetric Møller/Bhabha calorimeter at 1.29° and detector telescopes consisting of three triple GEM detectors interleaved with three MWPCs at 12° in both left and right sectors.

The following sections describe the detector components in greater detail.

4.1. Toroidal Magnet

The toroidal magnet consisted of eight copper coils placed around the beam line and scattering chamber so that the beam traveled down the toroid's symmetry axis (see Fig. 10). The coils divided the space around the beamline

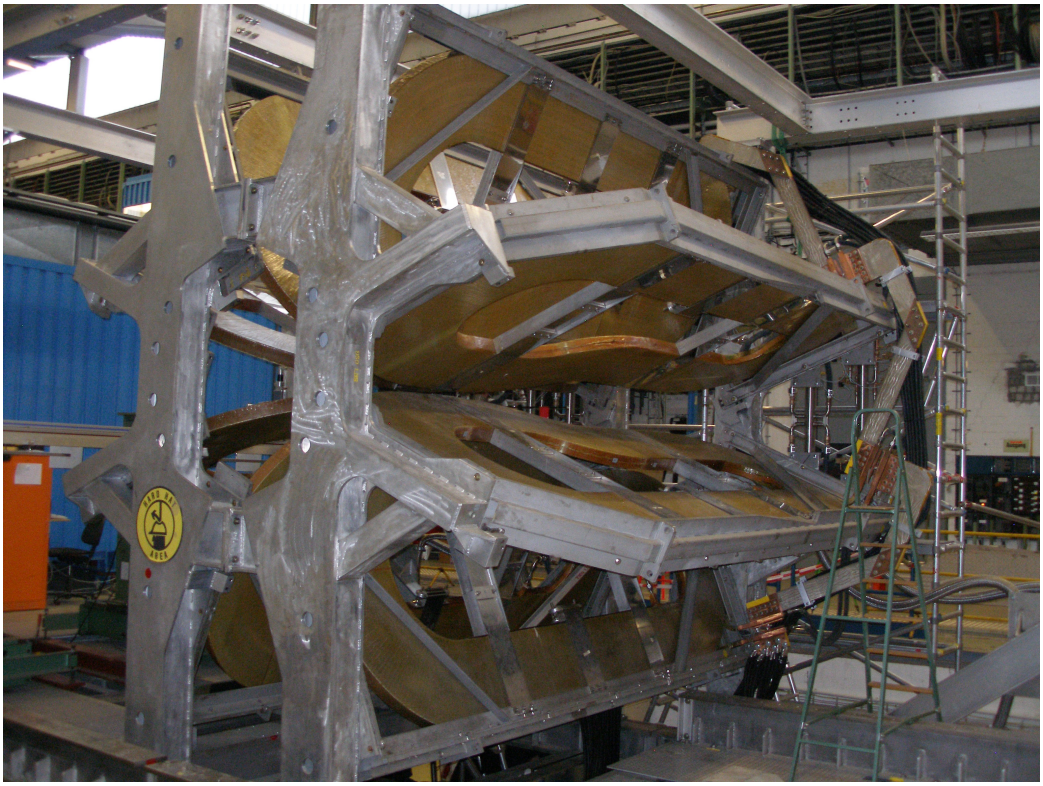

Fig. 10: The toroid magnet assembled at DESY before the subdetectors were installed

into eight sectors. The two sectors in the horizontal plane were instrumented with detectors. During normal operation, the magnet produced a field of about 0.28 T in the region of the tracking detectors.

The magnet was originally designed and used for the BLAST experiment, and has been described in previous article(15). The choice of a toroidal configuration was made to ensure a small field along the beamline, in order to minimize any effects on a spin-polarized beam, and to limit field gradients in the region of the polarized target. Since OLYMPUS used neither a polarized beam, nor a polarized target, these concerns were not as important. However, during the initial set-up, the magnetic field along the beamline was measured

and the coil positions adjusted to achieve an integrated field < 0.005 T·m to avoid perturbing the beam's position or direction.

Each of the toroid's eight coils consisted of 26 turns of 1.5 inch square copper tubes, organized into two layers of 13 turns. A circular hole, 0.8 inches in diameter, ran down the length of each tube and served as a conduit for cooling water. During assembly, the tubes were individually wrapped with fiberglass tape and then collectively potted in an epoxy resin matrix. The final outline and nominal position relative to the beam line and target center at the coordinate origin are shown in Fig. 11. The coils are narrower at one

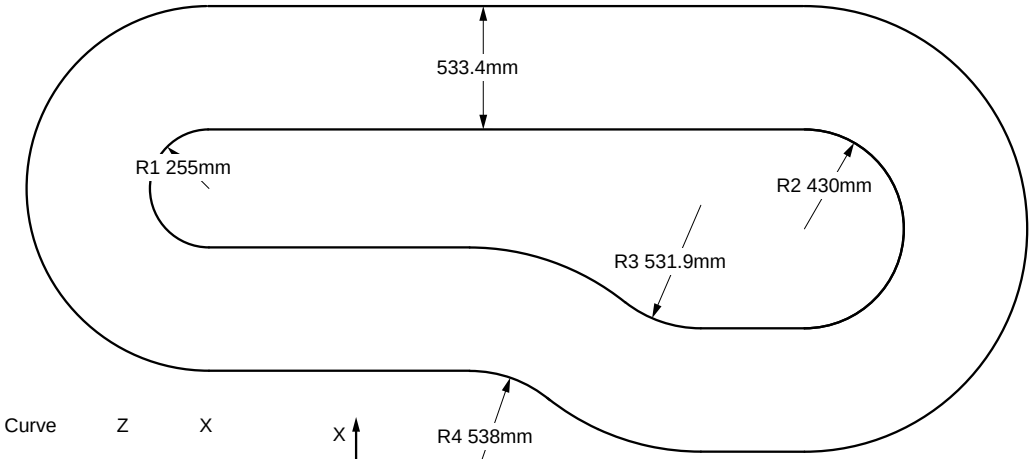

Curve	Z	X
R1	-636.3	1288.4
R2	1938.5	1113.4
R3	1491.0	1215.5
R4	491.0	-38.5

Fig. 11: Plan view of BLAST coil outline showing dimensions and position relative to the center of the target cell.

end to accommodate the scattering chamber and wider at the other to extend the high-field region to more forward angles, where scattered particles have higher momenta.

The magnetic field served two purposes. The first was to bend the tracks of charged particles, allowing their momentum and charge sign to be determined from the curvature of their tracks. The second was to sweep away low-energy, charged background particles from the tracking detectors. Though a stronger magnetic field would have improved momentum resolution and reduced the background, it would also have increased the Lorentz angle of drift electrons in the tracking detectors, making track reconstruction more

difficult. A balance was struck by choosing a current of 5000 A for normal operations, which produced a field of about 0.28 T in the high-field regions.

Originally, it was planned to alternate the polarity of the magnet every few hours, to reduce systematic uncertainties. However, this proved impractical at high-luminosity. In the negative polarity setting, the magnet bent negatively charged particles outward from the beamline. The drift chambers were hit with large background of low-energy electrons, which frequently caused the high-voltage supply to exceed its current threshold and deactivate. Attempts to adequately shield the drift chambers, both by adding material and by increasing the magnetic field strength, were unsuccessful. Consequently, the negative polarity setting was limited to low-luminosity running, and only about 13 % of the total luminosity was collected in this mode. The limited negative polarity data will be used to check systematic uncertainties.

After the experimental running period was completed, the drift chambers, the 12° luminosity monitors, the Møller detector, and the beamline downstream of the scattering chamber were removed in order to conduct a measurement of the magnetic field. The field region was scanned using a 3D Hall probe, mounted to a rod, driven by several translation tables. The rod was mounted to a long XYZ table with a range of motion of 0.2 m by 0.2 m by 6 m. (By convention, the direction of the beam was labeled as the OLYMPUS Z-axis, the Y-axis pointed up, and the X-axis pointed toward the left sector, forming a right-handed coordinate system.) This long table was supported by two large XY tables that augmented the X and Y ranges each by 1 m. The range of motion was further extended in X by substituting rods of different lengths and in Y by adding a vertical extension piece. The apparatus was used to measure the field over a grid of points on the left sector, before being transported and reassembled for a similar measurement of points on the right sector. The grid extended from -0.5 m to 3.5 m in Z. In X and Y, the grid was limited to the triangular space between the coils, but extended to ± 2.7 m on either side of the beamline. The grid points were spaced 0.05 m apart in the region within 1 m of the beamline, and 0.10 m apart in the outer region, where the field changed less rapidly. In total, approximately 35,000 positions were measured, including the downstream beamline region, which was measured redundantly from the left and the right.

After the initial setup of the apparatus, the precise position of the XYZ tables was measured with a laser tracking station over the course of a typical

scan in Z. This showed that the Hall probe position varied in X and Y as a function of Z during a scan, but that the shape was quite reproducible. To correct for this variation, the start and end points of each scan were measured using a theodolite and a total station. This data then allowed the position of the Hall probe to be determined for each measurement.

After correcting the Hall probe positions, a fit was performed to the magnetic field data. The fit was based on a model of the coil geometry with a Biot-Savart calculation of the magnetic field. The fit allowed the coil positions to vary slightly to best match the measurements. This model was then used to extrapolate the field over the entire volume around the OLYMPUS detector for use in track reconstruction and in the OLYMPUS Monte Carlo simulation.

4.2. Drift Chambers

The drift chambers used for the OLYMPUS experiment came from the BLAST experiment at MIT-Bates and have been described in great detail elsewhere (13), so the following description will be brief while mentioning new and updated features.

The drift chambers were used to measure the momenta, charges, scattering angles, and vertices of out-going charged particles. This was achieved by tracking those particles in three dimensions through the drift chambers, which were positioned within the toroidal magnetic field. Reconstructing a particle's trajectory backwards to the scattering vertex allowed the scattering angles and vertex position to be determined. Measuring the curvature of a trajectory yielded the particle's momentum, while the direction of curvature indicated the sign of particle's charge. The drift chambers had a large angular acceptance and nominally subtended a range of 20°–80° in polar angle and a $\pm 15°$ range in azimuth. The chambers were oriented to be normal to a polar angle of 73.54°. Because of these choices, the chambers were trapezoidal in shape (see Fig. 12).

The drift chambers were arranged in two sectors that were positioned on either side of the target, in the horizontal plane. Each sector contained three drift chambers (inner, middle, and outer) joined together by two interconnecting sections to form a single gas volume. Thus, only one entrance and one exit window were needed, reducing multiple scattering and energy loss. A cross sectional view of the top plate of one of the assembled gas volumes is shown in Fig. 13.

The drift chambers combined had approximately 10,000 wires used to create the drift field. Of these, 954 were sense wires, which read out the signals from ionization caused by a charged particle track. Because transporting the chambers in a way that would protect the wires from breaking was infeasible, the chambers were unstrung before being shipped from MIT-Bates to DESY. The chambers were then completely rewired in a clean room at DESY over a period of about three months during the summer of 2010. The wires were strung vertically between the top and bottom plates. Holes were machined in the thin sections of the recessed areas of the plates to accommodate Delrin feedthroughs. A hollow pin, made of gold-plated copper, was fixed in each feedthrough. Each wire was strung through a feedthrough and pin in the top and bottom plates. The pins were then crimped, fixing the wire in place and forming a good electrical contact between the wire and pin. High voltage was distributed to the wires via connectors that were soldered to the pins. In

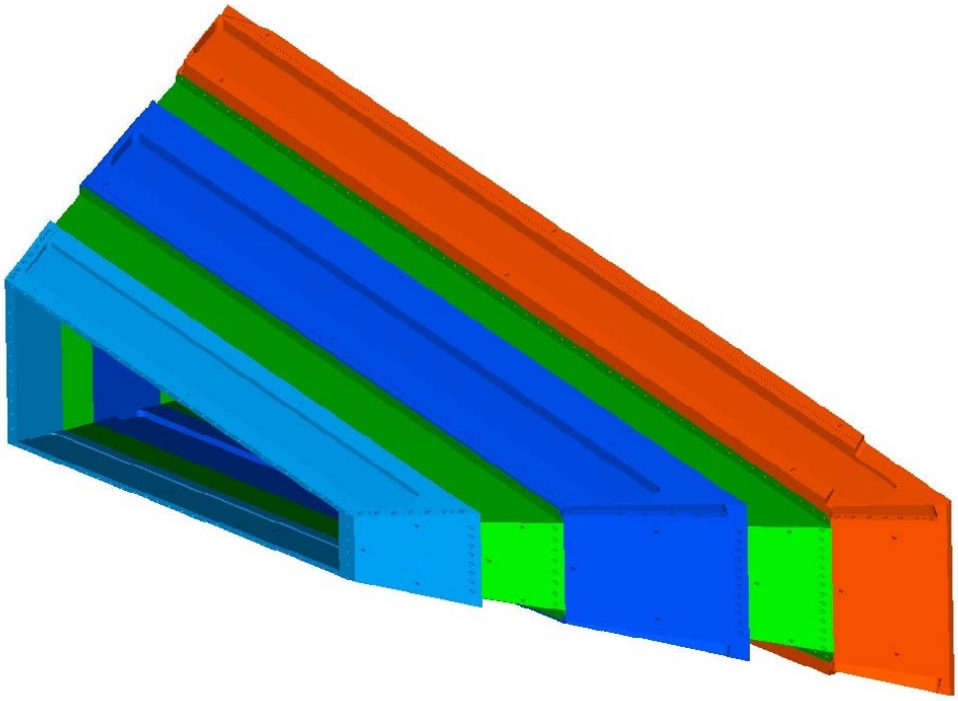

Fig. 12: Isometric view of all three drift chambers assembled into a single gas volume.

addition to new wires, improvements were made to the front-end electronics, building on experience gained from BLAST.

Each chamber consisted of two super-layers (or rows) of drift cells, with 20 mm separation between the super-layers. The drift cells were "jet-style," formed by wires. Fig. 14 shows a cross-sectional view of a portion of one chamber with the two super-layers of drift cells. It also shows characteristic "jet-style" lines of electron drift in a magnetic field. Each drift cell was 78×40 mm^2 and had 3 sense wires staggered ± 0.5 mm from the center line of each cell to help resolve the left/right ambiguity in determining position from the drift time. The wires in one super-layer were strung with a 10° stereo angle relative to wires of the other so that each chamber could localize a trajectory in three dimensions.

For the experiment an argon:carbon dioxide:ethanol gas mixture (90:10:3) was chosen for the drift chambers. The ethanol was added by bubbling the argon:carbon dioxide gas mixture through a volume of liquid ethanol kept at

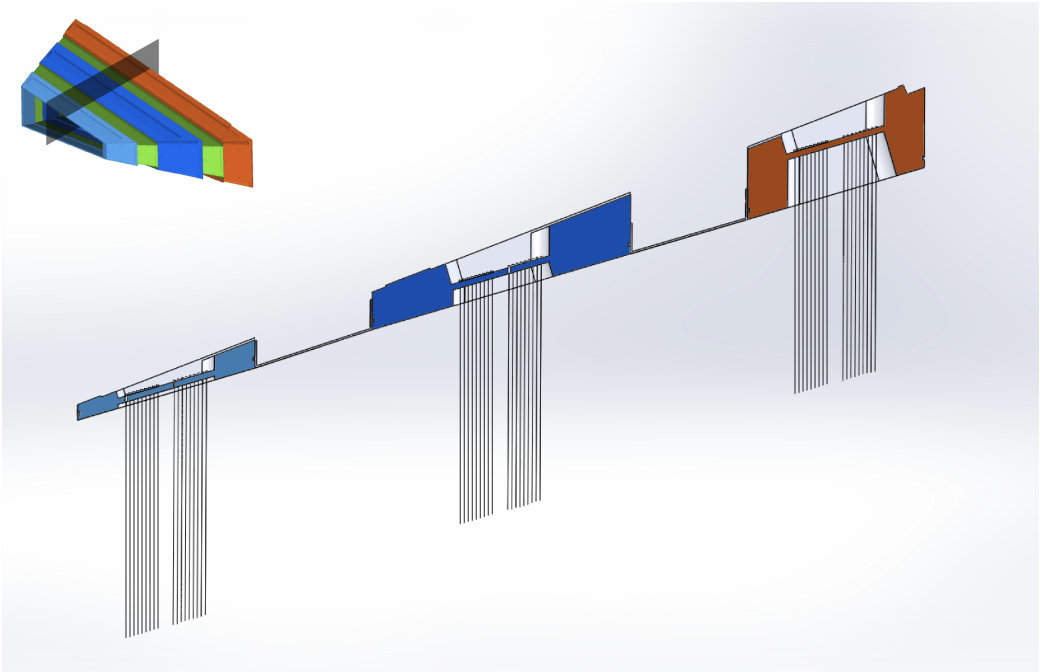

Fig. 13: Cross sectional view of the top plates of the three drift chambers and the two interconnecting sections when assembled into a single gas volume. The recesses between the top plates of the individual chambers housed front-end electronics and cables.

$\sim 5°$C. The chambers were maintained at a pressure of approximately 1 inch of water above atmospheric pressure with a flow rate of around 5 L/min.

Signals in the sense wires were processed with front-end electronics housed in the recesses of the interconnecting sections before being sent to TDC modules in the electronics hut. The signals were first decoupled from the high-voltage on new, custom-designed, high-voltage distribution boards. The signals next passed to Nanometrics Systems[6] N-277L amplifier/discriminators. Then the signals were passed by Ethernet cable to the electronics hut, to LeCroy[7] 1877 Multihit TDC modules, operated in common-stop mode, with the stop signal being provided by a delayed trigger signal. The digitized signals were fed into the data acquisition system.

[6]Nanometric Systems, Berwyn, IL, USA
[7]Teledyne Lecroy, Chestnut Ridge, NY, USA

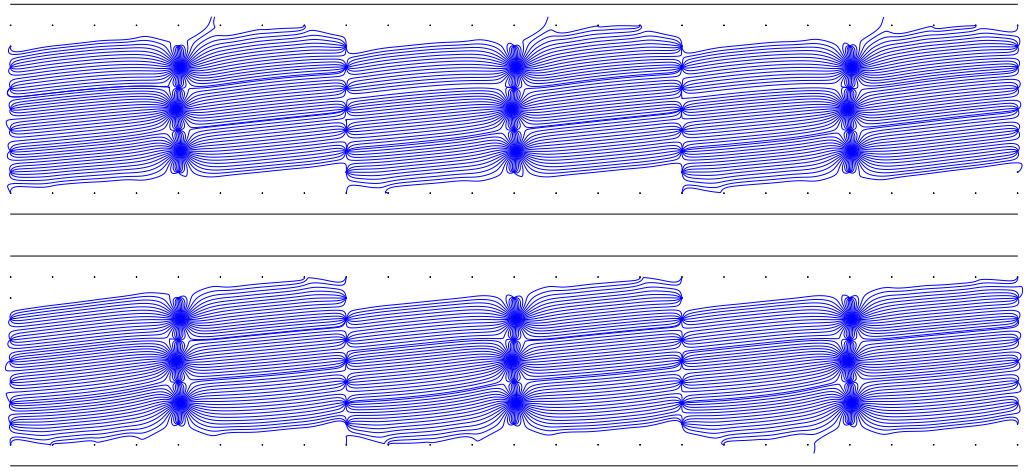

Fig. 14: Portion of a chamber showing the two super-layers of drift cells formed by wires. Lines of electron drift in the drift cells assuming a typical magnetic field around 3.0 kG are also shown.

4.3. Time of Flight Detectors

The time of flight, ToF, detector was from the BLAST experiment (13). The OLYMPUS experiment however did not use the Čerenkov detectors from BLAST. This allowed the ToF scintillators to be repositioned closer to the wire chambers and to add additional scintillator bars to improve the coverage. Each sector had 18 vertical scintillator bars with photo-multiplier readout at both ends as shown in Fig. 15. The forward four bars at were 119.4 cm high,

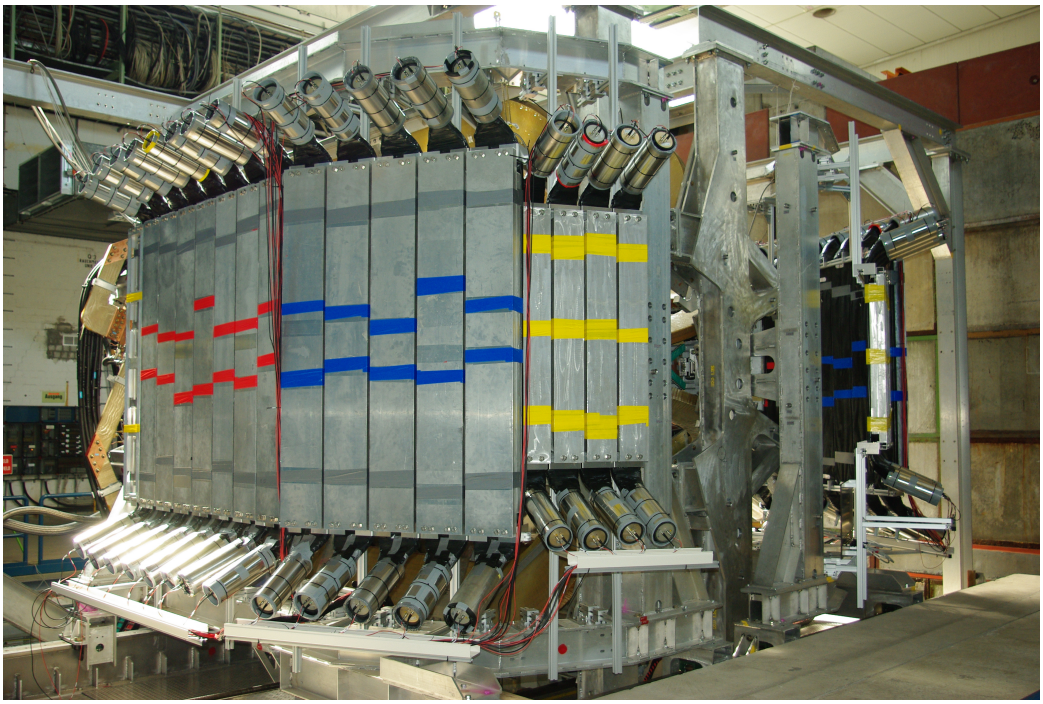

Fig. 15: ToF detector mounted in sub-detector support during assembly.

15.2 cm wide, and 2.54 cm thick. The remaining 14 bars were 180.0 cm high, 26.2 cm wide, and 2.54 cm thick.

The ToF detector provided a timing signal used to trigger the readout and data acquisition system for all other components and particularly provided the COMMON STOP signal for the drift chambers. The ToF readout consisted of ADCs and TDCs. The summed ADC signals from a given ToF bar gave a measure of energy deposited to aid particle identification. Approximate position information was also possible from the timing difference between the top and bottom photomultiplier tubes.

Bicron[8] BC-408 plastic scintillator was chosen for its fast response time (0.9 ns rise time) and long attenuation length (210 cm). Each ToF scintillator bar was read out at both ends via Lucite light guides coupled to 3-inch diameter Electron Tubes[9] model 9822B02 photomultiplier tubes equipped with Electron Tubes EBA-01 bases. The light guides were bent to point away from the interaction region so the PMTs would be roughly perpendicular to the toroidal magnetic field. Mu-metal shielding was used around all PMTs. The bases had actively stabilized voltage dividers so that the timing was independent of the gain.

To monitor the timing and amplitude of the ToF scintillator signals an LED based flasher system was designed and installed. The main component was an LED driver powering a type 7104 LED with wavelength 465 nm and brightness greater than 3000 mCd produced by KingBright. The light from the LED was divided into 36 optical fibers (TCU-1000W) with 1 mm of diameter. Each fiber was then connected to the center of each scintillator bar. A separate fiber was connected to a fast PIN photodiode to monitor the LED amplitude. The PMT signals had an amplitude of ~ 0.8 V with a rise time ~ 8 ns.

[8]Bicron, Solon, OH, USA

[9]Electron Tubes Ltd, Ruislip, Middlesex, England

5. Luminosity Monitors

In order to measure the ratio of differential cross sections for positron-proton and electron-proton elastic scattering it was essential to measure the luminosity for each run very precisely. In OLYMPUS there were three methods to track the luminosity:

- The slow control system monitored the beam current and gas flow to the target. Knowing the temperature of the target cell and its geometry a rough calculation could determine the target density. The product of target density and beam current could be integrated over a run to give a first estimate of the luminosity.

- The 12° luminosity monitors consisting of telescopes of 3 triple GEM detectors interleaved with 3 MWPCs and triggered by plastic scintillators could measure leptons scattered over a small angular range around 12° in coincidence with proton in the wire chambers. At small angles the two-photon contribution is expected to be small so this rate gives a measure of the luminosity.

- Finally a high precision measurement using symmetric Møller or Bhabha scattering was achieved using a $PbFl_2$ calorimeter at 1.292°.

Details on the last two luminosity monitoring system are provided in the next sections.

5.1. 12° *GEM Detectors*

Six planar triple-GEM detectors with 2D strip readout were built at Hampton University and installed as part of the 12° luminosity monitor together with the MWPCs. The GEM foils and 2D readout boards were produced by TechEtch, Inc.

The three tracking planes were located at distances of 187, 227, and 287 cm from the target, respectively, centered at 12° facing the target for perpendicular impact angle. Each telescope covered a solid angle of 1.2 msr, determined by the active area of 10×10 cm^2 and the distance of the farthest element of the telescope from the target.

The readout board had strips in the horizontal direction and pads in the vertical direction with a 400 micron pitch.

The front-end electronics was built by Rome.

5.1.1. 12° *Trigger*

Each 12° telescope had two $100 \times 100 \times 5$ mm^3 scintillator tiles with SiPM readout. These were used to provide a trigger signal.

A lead glass calorimeter consisting of four lead glass bars with PMT readout was mounted behind the telescope. This detector could also be used to provide a trigger and dedicated runs were made to measure the efficiency of the scintillator trigger.

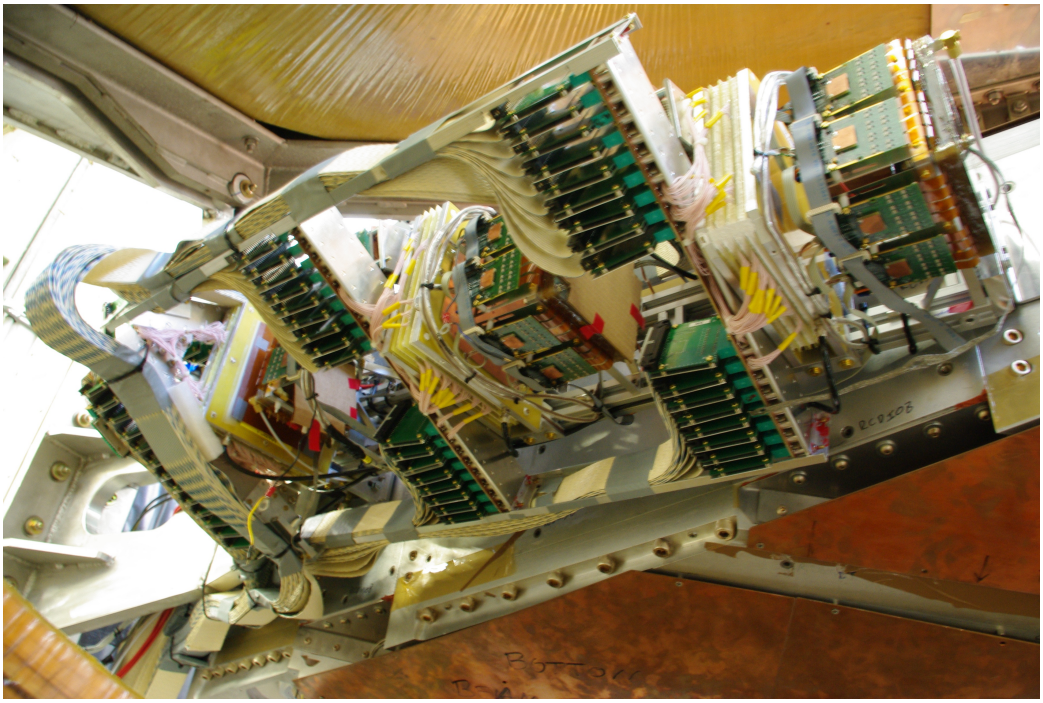

Fig. 16: Photograph of one of the 12° telescopes showing the GEM and MWPC detectors.

5.2. 12° *Multi-Wire Proportional Counters*

For the task of DORIS electron beam luminosity monitoring in OLYMPUS experiment it was proposed to use two blocks of MWPC (Multiwire Proportional Chambers). Each block of three MWPC is aligned along the axis going at the angle of 12° with respect to the interaction point at the left and right (creffig:12deg).

One MWPC module consists of three anode planes of sense wires U, X and V interleaved with the cathode wire planes. The sense wires have a 1 mm spacing and consists of 25 micron diameter gold-plated tungsten. The U and V wires are tilted by ±30° with respect to the vertical X wires. The cathode planes consist of 90 micron diameter beryllium bronze wires with 0.5 mm spacing. The general parameters for MWPC are presented in Table 1. Both anode and cathode electrode frames are made from fiberglass. These frames are sandwiched between two 10 mm thick aluminum frames.

The location of the MWPC blocks between the OLYMPUS magnet coils in vicinity of the beam pipe imposed several constrains on the detector modules design. Therefore the outer dimensions of the MWPC and positioning of

Active area	112×112 mm^2
External dimensions	$180 \times 180 \times 50$ mm^3
Anode planes	X ($0°$), U ($+30°$) and V ($-30°$)
Gap between anode and cathode	L=2.5 mm
Sense wire spacing	S=1 mm
Cathode wire spacing	S_{cath}=0.5 mm
Sense wire diameter	D=0.025 mm Au-plated tungsten
Cathode wire diameter	D_{cath}= 0.090 mm beryllium bronze
U, V angle wrt X wire	$\pm 30°$
MWPC material in acceptance	$\sim 0.25\%$
Working gas mixture	65%Ar+30%CO_2+5%CF_4
Gas gain at work point	$\sim 5 \times 10^4$

Table 1: Working parameters of MWPC module

the front-end CROS 3 readout electronics was simulated with GEANT3 and 3D CAD programs. This resulted in cut of frames corners from the beam pipe side on $\sim 8 \times 10$ mm^2. Front end electronic cards of the MWPC modules were aligned along the planes of the OLYMPUS magnet coils (Fig. 17).

As a working gas mixture MWPC use 65%Ar+30%CO_2+5%CF_4. This gas mixture was used for the magnet chambers(16) in the HERMES experiment and provided a stable operation of the detectors with good aging resistance. To evaluate high voltage working point for MWPC the gas gain dependence on applied high voltage was calculated using a GARFIELD program(17). Fig. 18 presents the calculated dependence of gas gain from the high voltage in 65%Ar+30%CO_2+5%CF_4 gas mixture. One can see that at HV=3150 V the gas gain reach about 5104. This simulation meets with results of the experimental measurements with produced in PNPI detectors. Eventually the working point at MWPC during the experiment was 3200 V.

The measuring of the MWPC operation with CROS3 electronic demonstrated a good performance of each MWPC block mounted in OLYMPUS magnet gap. Fig. 19 shows the wire map for the left (LM_L1-3(U,X,V)) and right (LM_R1-3(U,X,V)) detectors. A few channels were lost because of the contact imperfections in the cards connectors.

Track reconstruction is done using two different tracking algorithms. One method (TrackFitter) uses iterative procedure and GEANT4 tracking routine to match the track for given hit combination. Another method (KalmanFilter) uses Kalman filter algorithm for hit selection and track propagation in

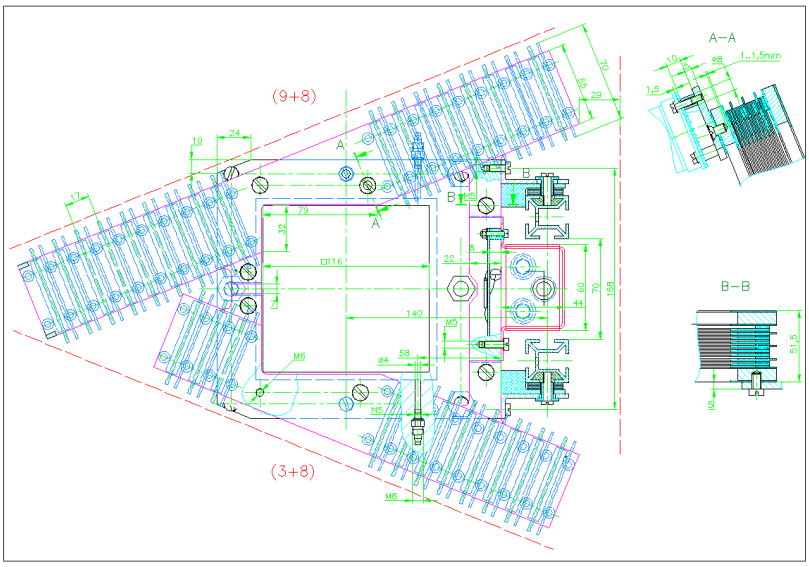

Fig. 17: Plan view of a MWPC detector assembly showing the square, active area in the center, the surrounding electronics, and the mounting fixtures.

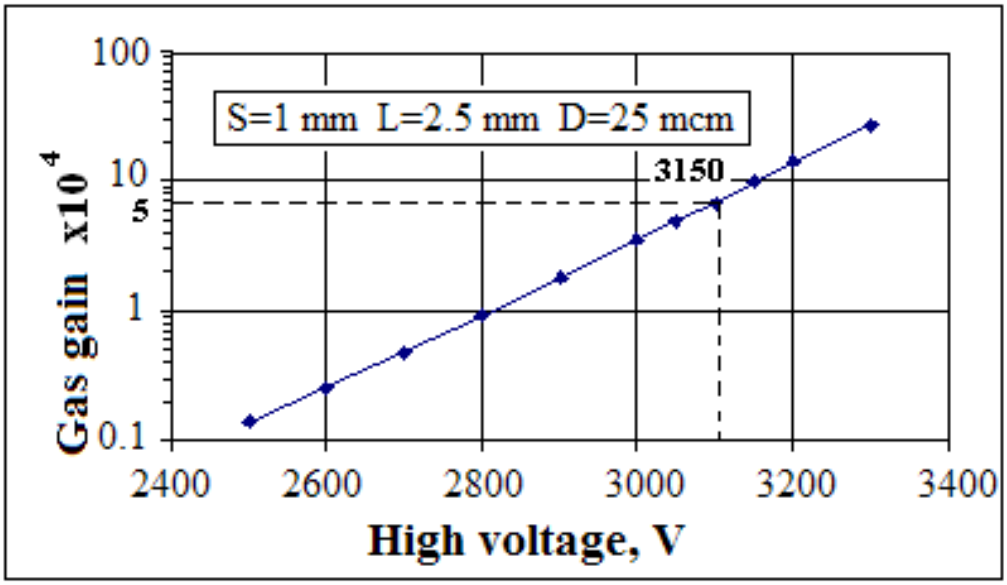

Fig. 18: Gas gain as a function of operating voltage for MWPC.

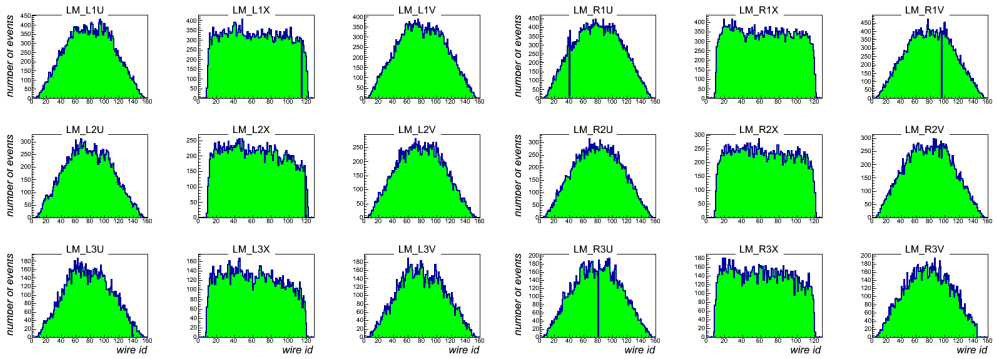

(a) Left MWPC telescope (b) Right MWPC telescope

Fig. 19: Wire hit distributions for the left and right MWPC telescopes showing the XUV planes for the three detectors.

magnetic field. Figure 5 shows charge lepton scattering angle (θ) for reconstructed tracks for various combination of the beam charge and magnet field direction. Even combination (++ or –) has a smaller average angle and correspondingly high cross section due to in-bending curvature then odd ones. Target density distribution along the beam is very well describe by primary vertices.

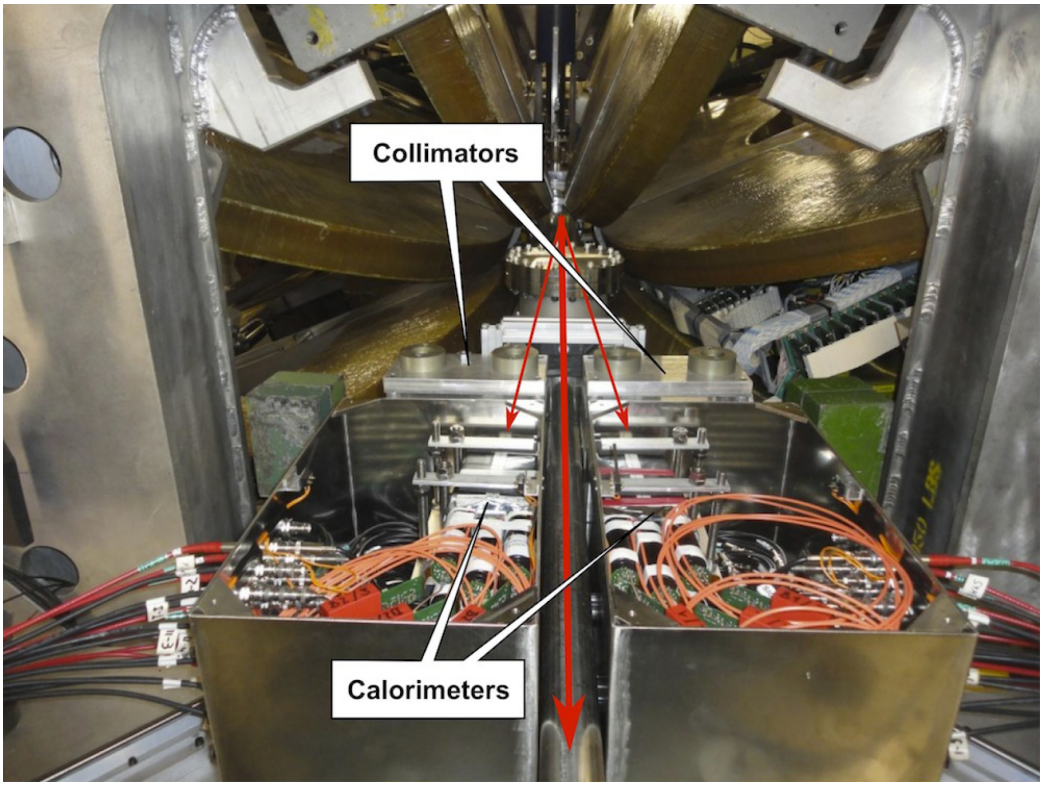

Fig. 20: The Symmetric Møller/Bhabha luminosity detector on the support table with the collimator in front of the μ-metal boxes.

5.3. Symmetric Møller/Bhabha Luminosity Monitor

The symmetric Møller/Bhabha luminosity detector (SYMB) was designed to monitor the luminosity by measuring symmetric lepton scattering $e^-e^- \to e^-e^-$ (Møller) and $e^+e^- \to e^+e^-$ (Bhabha) . For a beam energy of 2.01 GeV symmetric scattering occurs at a polar angle of 1.292° with respect to the incident beam direction. The cross sections for these processes can be precisely calculated from QED with the caveat that the annihilation reaction $e^+e^- \to 2\gamma$ must also be included with Bhabha scattering. By placing a pair of detectors at the symmetric angle (see Fig. 20) and measuring the coincident rates the luminosity could be determined.

The SYMB was build in Mainz and consisted of two symmetric 3×3 arrays of lead fluoride (PbF_2) crystals with photomultiplier readout (see Fig. 21). The tapered crystals were approximately $26 \times 26 \times 160$ mm^3. PbF_2 has a radiation length $X_o = 9.3$ mm and a Molière radius around 18 mm so the

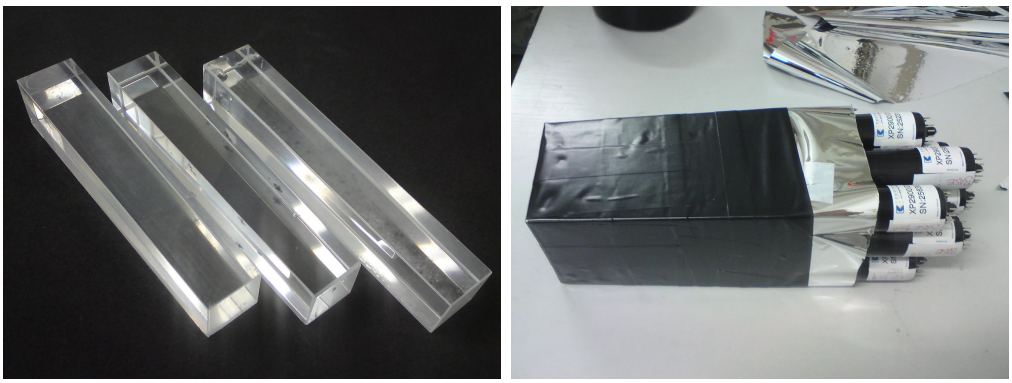

(a) PbF_2 crystals used in the symmetric Møller/Bhabha luminosity monitor.

(b) 3×3 array of wrapped PbF_2 crystals with PMT readout.

Fig. 21

3×3 array of crystals corresponded to ~ 17 radiation lengths longitudinal and ~ 2 Molière radii transversely sufficient to contain the electromagnetic shower within a very compact volume. PbF_2 is a pure Cerenkov detector with a very fast response ($\sim$ 20 ns) and no delayed components due to scintillation light. This enables the SYMB luminosity monitor to operate at the high rate expected at such a small angle. Each crystal was wrapped with Millipore paper to increase the reflectivity. The PMTs were Philips, model XP 29000/01. Each detector array was placed inside a μ-metal box to shield the photomultiplier tubes and the electronics from the magnetic field.

A thick lead collimator was placed upstream of the detector arrays to shield the crystals from Bremsstrahlung, Møller/Bhabha scattering at non-symmetric angles, and other background. The collimator had a removable central plug with a precision machined hole. This allowed the size of the collimator to be optimized more easily. For the OLYMPUS experiment a circular aperture with 20 mm diameter was chosen. This determined the solid angle subtended by each calorimeter. The location and angle of the collimator aperture was carefully surveyed before and after the experimental running periods and used in calculating the expected coincidence rates.

5.3.1. The data acquisition electronics

The electronics from the A4-experiment was used for the SYMB. This allowed a fast analogue summation of the signals from each crystal array with subsequent digitization and fast histogramming(18). The system had

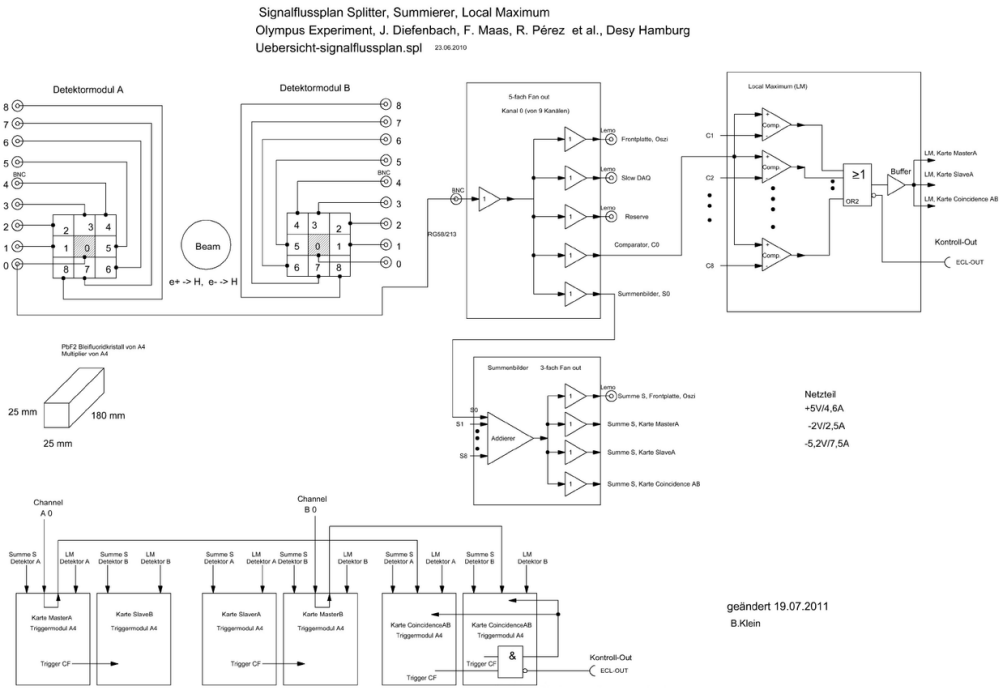

Fig. 22: The signal flow through the different tasks: input, trigger (local maximum), sum, digitize and storage in a histogram.

an overall dead time of 20 ns and allowed histogramming up to 50 MHz. The events lost at the expected Møller rate were estimated to be on the order of 1%.

The readout concept is show in Fig. 22. First the 9 analog signals from each crystal of one detector were summed. This sum was split into three output modes: coincidence mode, master mode, and slave mode. At the same time the 9 analog signals were compared to determine if the local maximum (LM), the center of the shower distribution, was in the center of the 3×3 cluster. If this was the case and the total deposited energy was over the threshold of a constant fraction discriminator (CFD), a trigger signal was generated. This trigger signal on the LM and the sum S were forwarded to the histogram cards. Since the very high event rate, the signal flow through different tasks: input, FAN out, trigger on local maximum (LM), sum S, digitalizes and storage in a histogram.

Møller, Bhabha and annihilation events had the same energy deposition

in both calorimeters, whereas most background events had a different energy deposition in the two calorimeters. Therefore, a trigger signal was produced when there were a coincident signals in both calorimeter detectors exceeding the threshold. As a cross check a trigger signal is also produce when only one calorimeter has a signal over threshold. These three trigger signals correspond to the three different data acquisition modes: coincidence mode and two Master-Slave mode.

6. Trigger

The trigger system was responsible for selecting events to be recorded by the data acquisition system. A field programmable gate array, FPGA, based in a VME crate was used to combine up to 16 input signals to form up to 16 parallel trigger conditions. Each trigger condition could be prescaled to reduce the number of events recorded for that trigger condition (usually high rate events or background). The output from the FPGA was 8 trigger types for recording the event. In addition scalers recorded the number of each signal received during a run both free running and gated by the DAQ livetime.

The trigger capable (fast) subdetectors for OLYMPUS consisted of the ToF scintillator bars and the 12° luminosity monitor. Coincidences between the top and bottom PMTs of each ToF scintillator bar were OR'ed together into groups for the left and right sectors. A coincidence of the left AND right ToF groups would produce a trigger as a potential elastic $e^{\pm}p \to e^{\pm}p$ events. A coincidence between an event in the 12° telescope and a ToF event in the opposing sector produced a lumi trigger. Other triggers for events with ToF hits only in one sector or in the 12° telescope without the opposing ToF hit were also collected but prescaled. These could be used for calibration and/or monitoring detector efficiencies.

In the February data run the luminosity and hence event rate was lower than expected. However, it was noticed that the number of good $e^{\pm}p$ events was a small fraction of the triggers. To improve this a second level trigger was introduced for the fall data run requiring a reasonable candidate track in the wire chambers in coincidence with the ToF events. The front-end cards used on the wire chambers produced an OR of all the sense wires connected to that card. Thus a signal from a given card corresponded to a potential hit in one of five drift cells in a well know location in each chamber. Logical combinations of these signals gave a good indication that a potential track was present. This reduced the false trigger rate by about a factor of 10 and was very important for the higher luminosity running later in 2012.

Additionally these signals were gated by the DORIS bunch clock to suppress uncorrelated background.

7. Data Acquisition System

The OLYMPUS data acquisition system, DAQ, utilized the framework developed for the Crystal Barrel experiment at the ELSA accelerator in Bonn.

This framework consisted of both hardware and software. It was a synchronous system meaning that each detector was read out at a common *Event* signal, so that the coherence of the taken data was ensured during acquisition. This approach had the drawback of increased complexity compared to to a free-running acquisition system but ensured concurrent data at runtime increasing the reliability of the system since faulty subdetectors were immediately noticed during data taking.

To achieve synchronous operation a hardware synchronization system, the *Syncsystem*, was implemented. This system worked in master/slave mode, which was reflected in its hardware components (see Fig. 23). The *Sync-*

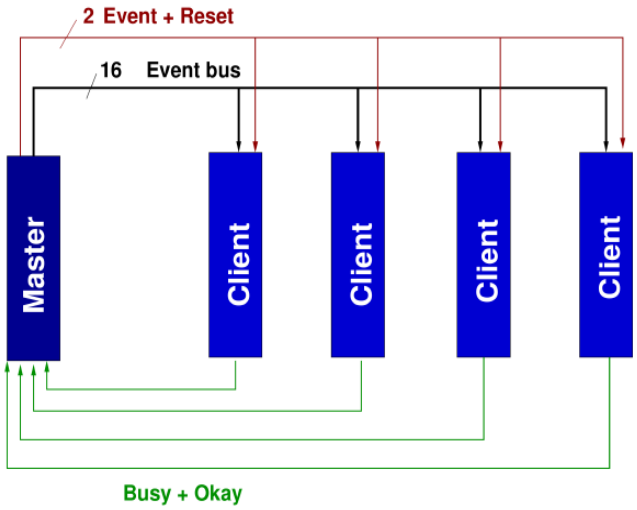

Fig. 23: Setup for synchronization.

Master was responsible for generating the *Event* signal which was then distributed to all clients. This system was implemented as 6U VME-Modules for both the *Sync-Master* as well as the *Sync-Clients*. Each of the modules was matched by a VME-CPU to perform the actual readout. Each *Sync-Client* signaled its state to the *Sync-Master* via its busy/okay lines, so that the master only generated an event if all clients were in a working state. Fig. 24 gives a detailed overview of such an synchronous event sequence.

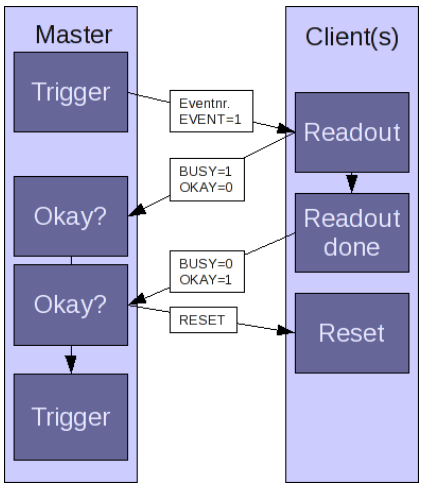

Fig. 24: Flow chart for synchronization.

The software side of this DAQ-framework was developed using the Linux operating system on x86-based VME-CPUs. It followed the concept of local eventbuilders (LEVB) for each subdetector (one CPU per subdetector but there could be more if required) and a global event builder which collected the data of each of the subsystems and checked it for completeness before committing the data to disk. For this it used two dedicated 1 GBit TCP/IP networks, one for control, the other for data transfer, minimizing bandwidth contention. Each LEVB was paired with a *Sync-Client* and interacted with it during readout. It provided all necessary building blocks to implement the sync scheme described above as well as the data transport via TCP/IP to the global event builder. As a consequence only the readout functions for the TDC, ADC, and scaler modules had to implemented, significantly lowering development time and required manpower. The global event builder featured a pluggable output system enabling a wide variety of data formats (the current version uses CERN ZEBRA) and could therefore be adapted to analysis needs of OLYMPUS. The achievable event rate of this system was about 30 kHz which was well above the limits imposed by the Fastbus modules, which have a maximum of about 1.5 kHz, making it perfectly suitable for OLYMPUS.

This system proved its reliability at the Crystal Barrel experiment over the last 6 years and is still being actively improved. All hardware used in this system is either developed in Bonn by members of the OLYMPUS

collaboration or readily commercially available making it future proof for the upcoming experiment. To implement this system a number of purchases have to be made especially for the CPUs and Sync-system. The existing BLAST CPUs cannot be reused since they have a different architecture making it unfeasible to port the software stack described above.

7.1. Graphical user interface

Using this existing system also provided additional benefits like a graphical run control system (see Fig. 25) which featured an integrated run database

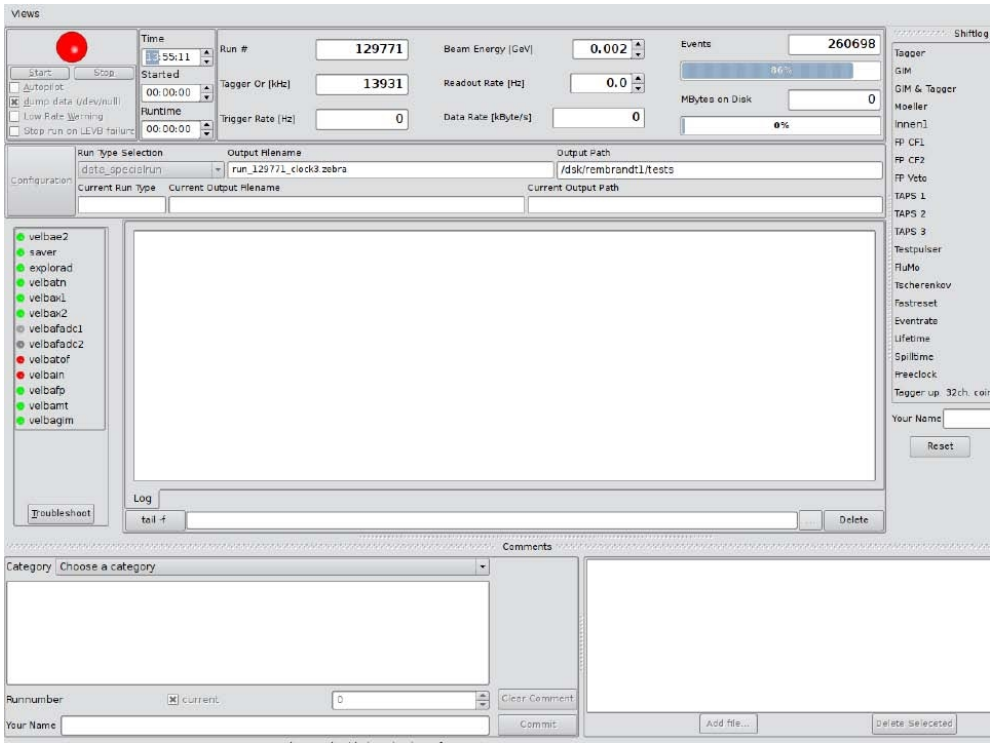

Fig. 25: Graphical run control system

accessible via web interface (see Fig. 26). This database tracked all relevant run parameters and included an online shift log which allowed to store e.g. comments of the shift crew correlated with the current run.

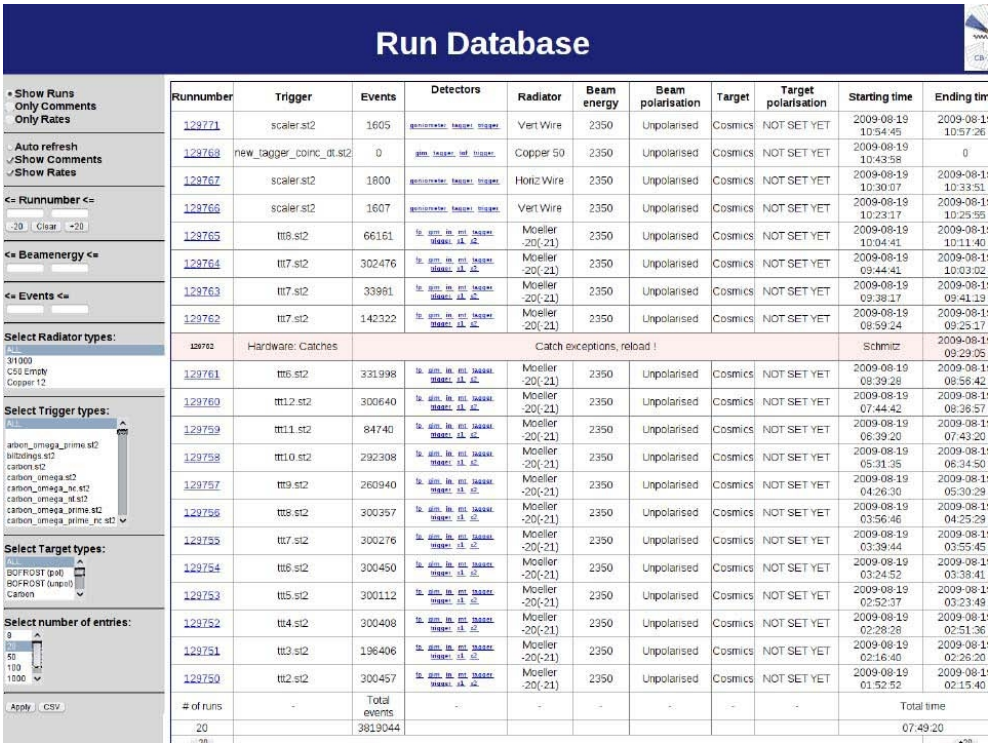

Fig. 26: Graphical interface to the run database

8. Slow Control

In addition to the detector electronics, trigger, and data acquisition system, successful operation of the OLYMPUS experiment required that hundreds of other components could be controlled, monitored, and recorded. These included the high voltages for the detectors, temperatures, pressures, flow rates and valves for the various detector gas systems as well as for the target and vacuum systems and numerous parameters concerning the beam (current, position, lifetime).

The Experimental Physics and Industrial Control System, EPICS[10], was used as the back-end solution. It was deployed on three Linux machines: two VME computers with interface cards to control equipment and one server which communicated with the database and was the interface to the DORIS control system.

A PostgreSQL database stored the current status of all parameters as well as their history. The same data were also mixed into the DAQ data stream which was saved to disk.

The slow control system had a user friendly graphical user interface (GUI) using a web application, based on Flask as middleware. In contrast to more standard solutions which typically involve the deployment of custom, operating system dependent programs to any control computer, the use of web technology made it possible to have concurrent view-only and control access from any Internet-ready computer. In addition to displaying the various parameters, the simple GUI allowed to change the settings to turn detectors on or off, raise or lower high voltages, change gas flows, open or close valves, etc. The system also provided alarm features to alert the shift crew if anything was not within a predetermined range.

[10] http://www.aps.anl.gov/epics/index.php

9. Operation

During normal data-taking runs, a two-person shift crew operated the OLYMPUS detector and monitored the quality of the data using a number of plots generated in near real-time. Typically, production runs were taken 24 hours a day during the February and fall runs, alternating daily between positron and electrons beams.

9.1. Data Collection

As previously noted in Sec. 2, the experiment employed two modes of operation separated by the manner in which the DORIS beam was operated. During the February run, the experiment was operated in "manual" mode in which the beam was initially filled to ~ 65 mA and then data was taken as the beam decayed to ~ 40 mA. At this point, the shift crew used the slow control interface (Sec. 8) to lower the high voltage of the various detectors to preset safe values. Since beam refills during the earlier running period were not as clean (more instability and losses), the lowering of the voltages prevented high voltage trips and possible damage to the detectors due to high rates during the refill. After lowering the voltages, the OLYMPUS shift crew informed the DORIS accelerator crew that the detector was ready for beam refill. Once the beam was restored to the normal starting current, the voltages were brought back to operational values and data-taking was restarted. During this mode of operation, a "run" dataset consisted of the data collected between such refills.

Between the February and fall runs, significant improvements were made to the DORIS beam injection process that allowed the OLYMPUS Experiment to be run in "top-up mode". In this mode, the beam was initially filled to ~ 6 mA as in the manual mode, but was only allowed to decay to ~ 58 mA before triggering an automatic refill. Due to the improved injection, it was not necessary to lower the high voltage of the OLYMPUS detectors during these injections. The DAQ was configured to briefly inhibit data-taking during injection pulses (see Sec. 2). This mode of running significantly increased the average instantaneous luminosity delivered to the experiment and freed the OLYMPUS shift crew to more carefully monitor the quality of the beam and incoming data.

Due to the importance of collecting data with both positrons and electrons, the beam species was switched each morning (with occasional exceptions for maintenance, evening-out the amount of data collected with each

species, etc.). This ensured that there were no systematic differences between e^+ and e^- runs introduced by environmental factors such as day/night cycles, reduced traffic on the DESY campus on weekends, etc. Similarly, during the February run, in which both toroid polarities were used, data-taking was segmented into four six-hour blocks each day. The toroid polarity in each block was selected by coin-toss (ensuring two blocks of each polarity per day).

In addition to production runs, empty target runs (with the H_2 gas flow shut-off and the target chamber pumped down to ring vacuum levels), zero magnetic field runs, and other test runs were taken on an approximately daily basis for the purposes of monitoring backgrounds, providing data for detector calibrations, and testing proposed changes to operations. When the DORIS beam was unavailable due to problems or maintenance, the detector was left active to collect cosmic ray data. Also, cosmic ray data was collected for approximately one month following the end of OLYMPUS productions runs in January 2013. This large cosmic data set will be used for various studies of detector efficiencies and calibration.

9.2. Data Quality Monitoring

During data-taking, the quality of the incoming data was monitored in several stages. Real-time, online monitoring of essential parameters was implemented using the ExPlORA framework originally developed by the Crystal Barrel collaboration (19). The ExPlORA program processed the raw data ZEBRA files as data was being taken to produce a variety of histograms and plot of quantities versus time, such as the number of drift chamber wires hit per event, ADC and TDC distributions, DAQ deadtime, and various detector rates. The OLYMPUS shift crew had access to reference plots corresponding to those shown in ExPlORA that showed data of known good quality and data representing known possible issues. This provided the shift crew with the ability to quickly identify problems with detectors as well as problems caused by poor beam quality and take action to resolve them rather than taking low-quality data.

For the fall run, a second level of data quality monitoring by the shift crew was implemented that allowed inspection of the data in a more processed format approximately 30 minutes after the conclusion of a single data run. This program automatically ran basic analysis programs on complete datasets as they became available and presented the data to the shift crew. Similarly to the real-time monitoring, this program presented histograms and plots of the recent data to be compared with data of known quality, but included

higher-level information such as the properties of events with good particle track candidates and basic measures of detector efficiencies.

Additionally, the longterm performance of the detector was monitored using the PostgreSQL database discussed in Sec. 8. This provided the ability to monitor the behavior of many detector parameters over the course of the entire data-taking period to identify slow drifts and sudden changes that could affect the analysis.

10. Summary

In 2012 the OLYMPUS experiment successfully collected approximately 4.35 fb^{-1} of data for electron and positron elastic scattering from hydrogen at the DORIS storage ring at DESY. A large acceptance, left/right symmetric detector system based on a toroidal magnetic spectrometer with drift chambers for tracking, time-of-flight scintillators for triggering and relative timing, and a redundant set of luminosity monitors was used. A flexible trigger and data acquisition system was used to collect the data. The experiment was explicitly designed and operated to minimize systematic errors by being left/right symmetric and changing beam species daily. The initial plan to change the toroidal magnet polarity daily was not possible because of high background rates with negative polarity. Consequently 78% of the data was collected with positive magnet polarity and the balance with negative polarity.

This paper has provided a technical description of the accelerator, internal target, detector, electronics, and operation of the OLYMPUS experiment. Future papers will detail the analysis and physics results obtained.

11. Acknowledgments

The successful design, construction, and operation of the OLYMPUS experiment would not have been possible without the research and technical support staffs of all the institutions involved. In particular we would like to acknowledge the DORIS accelerator group for providing the high quality electron and positron beams delivered to the experiment. We also gratefully acknowledge the DESY MEA and MKK groups for providing the necessary infrastructure and support during the assembly, commissioning, operation, and disassembly of the experiment. The research and engineering group from MIT-Bates was invaluable in all phases of the experiment from disassembling BLAST and shipping it to DESY through installation of OLYMPUS over numerous unanticipated problems and solution particularly with target and vacuum systems.

We would like to thank E. Steffens for numerous suggestions and helpful discussions during the initial development of the experiment.

Final we grateful acknowledge the DESY directorate, particularly Prof. Heuer and Prof. Mnich, and the DESY Physics Review Committee for their support, advice, and encouragement from the start of the proposal.

This work was supported by the US Department of Energy and the Russian Federal Ministry for Science and Education.

Appendix A. Kinematics

Some plots of kinematics relevant to the OLYMPUS experiment and elastic lepton-proton scattering at a beam energy of 2.01 GeV are given below. The straight lines indicate the nominal angular coverage of the wire chambers, 20°–80°, and the centerline of the 12° detector telescopes.

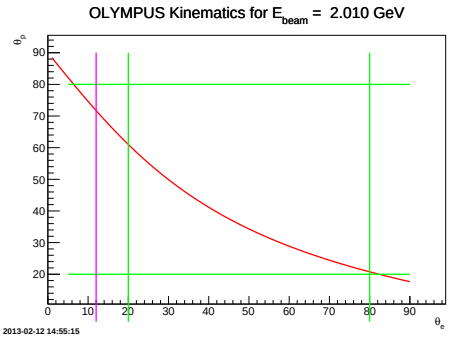

(a) Proton versus lepton scattering angle.

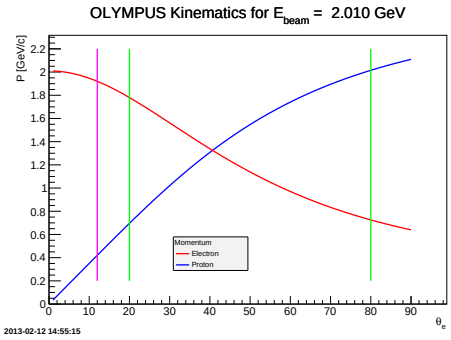

(b) Electron and proton momenta.

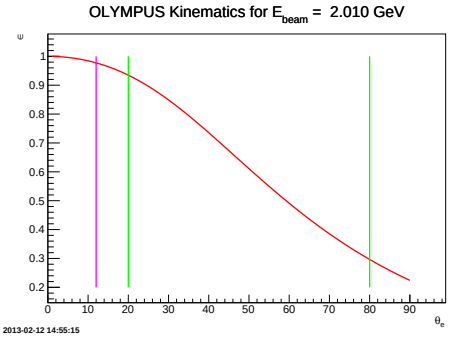

(c) Epsilon

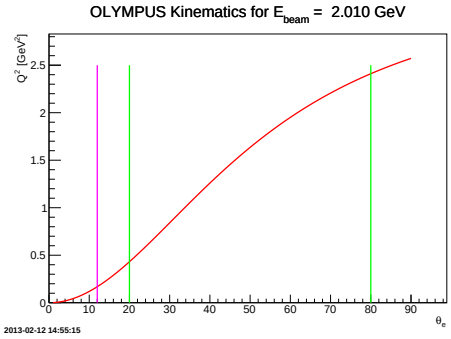

(d) Q^2

Fig. A.27

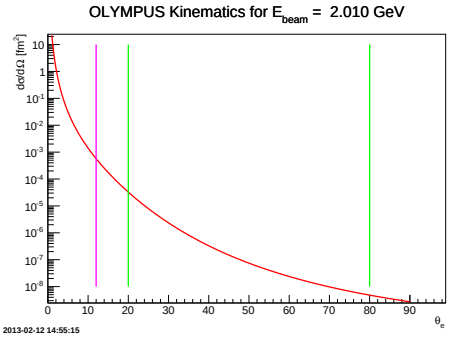

(e) Elastic *ep* cross section assuming dipole form factors.

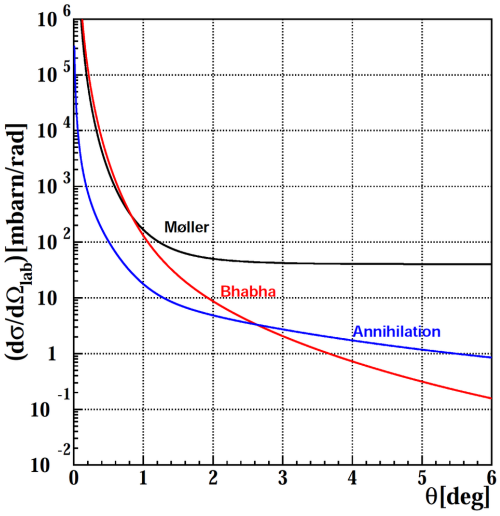

(f) Symmetric Møller, Bhabha, and annihilation cross sections.

Fig. A.27

References

[1] A. J. R. Puckett, others, Recoil Polarization Measurements of the Proton Electromagnetic Form Factor Ratio to $Q^2 = 8.5$ GeV^2, Phys.Rev.Lett. 104 (2010) 242301.

[2] M. Paolone, S. P. Malace, S. Strauch, I. Albayrak, J. Arrington, others, Polarization Transfer in the ^{4}He$(\vec{e}, e'\vec{p})^3$H Reaction at Q^2= 0.8 and 1.3 (GeV/c)^2, Phys.Rev.Lett. 105 (2010) 072001.

[3] B. Hu, others, Polarization transfer in the ^{2}H$(\vec{e}, e'\vec{p})n$ reaction up to Q^2 = 1.61 (GeV/c)^2, Phys.Rev. C73 (2006) 064004.

[4] M. K. Jones, others, G_{E_p}/G_{M_p} Ratio by Polarization Transfer in $\vec{e}p \to e\vec{p}$, Phys.Rev.Lett. 84 (2000) 1398–1402.

[5] G. MacLachlan, others, The ratio of proton electromagnetic form factors via recoil polarimetry at $Q^2 = 1.13$ (GeV/c)^2, Nucl.Phys. A764 (2006) 261–273.

[6] V. Punjabi, others, Proton elastic form factor ratios to $Q^2 = 3.5$ GeV^2 by polarization transfer, Phys.Rev. C71 (2005) 055202.

[7] S. Strauch, others, Polarization Transfer in the ^{4}He$(\vec{e}, e'\vec{p})^3$H Reaction up to $Q^2 = 2.6$ (GeV/c)^2, Phys.Rev.Lett. 91 (2003) 052301.

[8] O. Gayou, others, Measurement of G_{E_p}/G_{M_p} in $\vec{e}p \to e\vec{p}$ to Q^2 = 5.6 GeV^2, Phys.Rev.Lett. 88 (2002) 092301.

[9] I. A. Qattan, others, Precision Rosenbluth measurement of the proton elastic form factors, Phys.Rev.Lett. 94 (2005) 142301.

[10] M. E. Christy, others, Measurements of electron-proton elastic cross sections for $0.4 < Q^2 < 5.5$ (GeV/c)^2, Phys.Rev. C70 (2004) 015206.

[11] L. Andivahis, others, Measurements of the electric and magnetic form factors of the proton from Q^2= 1.75 to 8.83 (GeV/c)^2, Phys.Rev. D50 (1994) 5491–5517.

[12] R. C. Walker, B. W. Filippone, J. Jourdan, R. Milner, R. McKeown, D. Potterveld, L. Andivahis, R. Arnold, D. Benton, P. Bosted,

G. deChambrier, A. Lung, S. E. Rock, Z. M. Szalata, A. Para, F. Dietrich, K. Van Bibber, J. Button-Shafer, B. Debebe, R. S. Hicks, S. Dasu, P. de Barbaro, A. Bodek, H. Harada, M. W. Krasny, K. Lang, E. M. Riordan, Measurements of the proton elastic form factors for $1 \leq Q^2 \leq 3$ $(\mathrm{GeV/c})^2$ at SLAC, Phys. Rev. D 49 (11) (1994) 5671–5689.

[13] D. Hasell, T. Akdogan, R. Alarcon, W. Bertozzi, E. Booth, others, The BLAST experiment, Nucl.Instrum.Meth. A603 (2009) 247–262.

[14] H. Albrecht, others, Physics with ARGUS, Phys.Rept. 276 (1996) 223–405.

[15] K. A. Dow, T. Botto, A. Goodhue, D. K. Hasell, D. Loughnan, others, Magnetic field measurements of the BLAST spectrometer, Nucl.Instrum.Meth. A599 (2009) 146–151.

[16] A. Andreev, S. Belostotsky, G. Gavrilov, O. Grebenyuk, E. Ivanov, others, Multiwire proportional chambers in the HERMES experiment, Nucl.Instrum.Meth. A465 (2001) 482–497.

[17] R. Veenhof, GARFIELD, recent developments, Nucl.Instrum.Meth. A419 (1998) 726–730.

[18] R. Kothe, Design and operation of fast calorimeter electronics for an experiment for the measurement of the parity violation in elastic electron scattering.

[19] D. M. Piontek, The new online monitor for the Crystal Barrel Experiment at ELSA, 24th Students' Workshop on Electromagnetic Interactions Bosen (Saar), 2006.